# Inhibition of CXCR2 profoundly suppresses inflammation-driven and spontaneous tumorigenesis

Thomas Jamieson,[1] Mairi Clarke,[2] Colin W. Steele,[1] Michael S. Samuel,[1] Jens Neumann,[3] Andreas Jung,[3] David Huels,[1] Michael F. Olson,[1] Sudipto Das,[2] Robert J.B. Nibbs,[2] and Owen J. Sansom[1]

[1]Beatson Institute of Cancer Research, Glasgow, United Kingdom. [2]Institute of Infection, Immunity and Inflammation, College of Medical, Veterinary and Life Sciences, University of Glasgow, Glasgow, United Kingdom. [3]Pathologisches Institut, Ludwig-Maximilians Universität München, Munich, Germany.

**The chemokine receptor CXCR2 is a key mediator of neutrophil migration that also plays a role in tumor development. However, CXCR2 influences tumors through multiple mechanisms and might promote or inhibit tumor development depending on context. Here, we used several mouse models of spontaneous and inflammation-driven neoplasia to define indispensable roles for CXCR2 in benign and malignant tumors. CXCR2-activating chemokines were part of the secretome of cultured primary benign intestinal adenomas ($Apc^{Min/+}$) and highly expressed by all tumors in all models. CXCR2 deficiency profoundly suppressed inflammation-driven tumorigenesis in skin and intestine as well as spontaneous adenocarcinoma formation in a model of invasive intestinal adenocarcinoma ($AhCreER;Apc^{fl/+};Pten^{fl/fl}$ mice). Pepducin-mediated CXCR2 inhibition reduced tumorigenesis in $Apc^{Min/+}$ mice. Ly6G$^+$ neutrophils were the dominant source of CXCR2 in blood, and CXCR2 deficiency attenuated neutrophil recruitment. Moreover, systemic Ly6G$^+$ cell depletion purged CXCR2-dependent tumor-associated leukocytes, suppressed established skin tumor growth and colitis-associated tumorigenesis, and reduced $Apc^{Min/+}$ adenoma formation. CXCR2 is thus a potent protumorigenic chemokine receptor that directs recruitment of tumor-promoting leukocytes into tissues during tumor-inducing and tumor-driven inflammation. Similar leukocyte populations were also found in human intestinal adenomas, which suggests that CXCR2 antagonists may have therapeutic and prophylactic potential in the treatment of cancer.**

## Introduction

Inflammation and tumorigenesis are intimately linked. Chronic inflammation can drive tumorigenesis, and tumors are inherently proinflammatory, with infiltrating leukocytes thought to be critical for tumor maintenance and progression (1, 2). In colorectal cancer, for example, ulcerative colitis increases risk greater than 20-fold (3); NSAIDs reduce it by approximately 50% (4); and inflammatory infiltrate profiles predict patient outcome (5). Molecules that drive tumor-driven, or tumor-inducing, inflammation have considerable potential as therapeutic targets. Among these are inflammatory chemokine receptors, heptahelical G protein–coupled receptors that mediate the biological effects of secreted inflammatory chemokines. They are key regulators of inflammation in a spectrum of physiological and pathological contexts. Established cancers often constitutively produce a subset of proinflammatory chemokines, which, through multiple chemokine receptors, are thought to shape leukocyte infiltrate, regulate other stromal cells, and, in some instances, directly control tumor cells (6). However, the overlapping chemokine binding profiles of inflammatory chemokine receptors means that it may not be possible to identify individual chemokine receptors with sufficiently profound effects on de novo tumor development to represent realistic targets for cancer therapy or prophylaxis.

Chemokines that activate the chemokine receptor CXCR2 are expressed by a wide variety of established human cancer types. The chemokines CXCL1, CXCL2, CXCL3, CXCL5, CXCL6, CXCL7, and CXCL8 all activate human CXCR2; CXCL6 and CXCL8 also signal through human CXCR1 (7). Although mouse CXCR2 binds a similar spectrum of chemokines, mice lack *Cxcl8*; they have only 1 CXCL5/6-like gene (referred to herein as *Cxcl5*); and their *Cxcl2* and *Cxcl3* genes are highly homologous and coregulated. Mouse *Cxcl5* also binds mouse CXCR1 (8), although the function of this receptor in vivo is unclear. Neutrophils, readily identified by expression of Ly6G (a component of the Gr1 epitope), are the predominant CXCR2$^+$ cells among blood leukocytes, and CXCR2 is a key regulator of their recruitment and effector responses (7, 9). Depending on the context, both pro- and antitumor activities have been attributed to neutrophils (10). CXCR2 is also expressed by neutrophil precursors in the bone marrow that can be released during systemic inflammation, and by many Gr1$^+$CD11b$^+$ cells in tumor-bearing mice, a population that likely includes neutrophils, their precursors, and polymorphonuclear myeloid-derived suppressor cells (MDSCs) (11, 12). CXCR2 can also be found on endothelial cells (13), where it can mediate angiogenesis (14) and augment neutrophil recruitment (15). It is also seen on some tumor cells and can be induced by activated oncogenes (e.g., ras) (16). Its function on transformed cells is context dependent. For example, CXCR2 is required for the optimal growth of ras-transformed keratinocytes in vivo (17) and has been shown to stimulate tumor cell growth, survival, and motility in several model systems (18–20). In contrast, induction of CXCR2 and its

**Authorship note:** Thomas Jamieson and Mairi Clarke contributed equally to this work. Robert J.B. Nibbs and Owen J. Sansom are co–senior authors.

**Conflict of interest:** The authors have declared that no conflict of interest exists.

**Citation for this article:** *J Clin Invest.* 2012;122(9):3127–3144. doi:10.1172/JCI61067.

ligands by oncogenic K-ras reinforces senescence in vitro (21), predicting a role in tumor suppression in vivo. In some cancers, such as prostate cancer, CXCR2 is expressed by early premalignant cells, but downregulated during tumor progression (21–23).

Collectively, these observations — many of which have come from studying cell lines in culture or transplanted into mice — suggest that CXCR2, operating on multiple cell types, could have positive and negative influences on cancer initiation, development, and invasion. Since CXCR2 inhibitors are under development for the treatment of a variety of inflammatory disorders (24, 25), it is critical that the overall role of CXCR2 during tumorigenesis in multiple tissues is fully understood. If CXCR2 is protumorigenic, these inhibitors may be efficacious for cancer chemoprevention or therapy. However, their use to treat inflammatory disease might be inadvisable if CXCR2 acts as a tumor suppressor by, for example, blocking progression of premalignant lesions. Although it has been previously shown that CXCR2 antagonism does not inhibit mouse mammary adenocarcinoma growth, despite partially reducing $Gr1^+CD11b^+$ cell abundance in the tumor (11), recent work has shown that pancreatic ductal adenocarcinoma progression can be suppressed using a CXCR2 inhibitor (26), and *Cxcr2*$^{-/-}$ mice are reportedly less susceptible to skin and prostate tumorigenesis (27, 28). Here, using inflammation-driven and spontaneous mouse models of intestinal and skin neoplasia, including benign and malignant tumor models, we reveal how *Cxcr2* deficiency and/or inhibition, or CXCR2-expressing $Ly6G^+$ cell depletion, resulted in profound suppression of tumorigenesis. We propose that CXCR2 antagonists may therefore have potential as novel prophylactic or therapeutic anticancer treatments.

## Results

*CXCR2 is expressed by blood- and tumor-associated Gr1*$^+$ *cells, and its chemokine ligands are constitutively produced by papillomas*. Topical treatment of susceptible mice with 7,12-dimethylbenz[α]anthracene (DMBA), followed by repeated application of 12-*O*-tetradecanoyl phorbol-13-acetate (TPA), generates inflammation-driven premalignant lesions that express high levels of senescence markers (21, 29). Several weeks after the last TPA application, substantial numbers of cells adjacent to, and within, these tumors expressed myeloperoxidase (MPO) (Figure 1A), a marker of neutrophils and some MDSCs. We were interested in identifying the chemokine receptor that might be responsible for the recruitment of these cells. CXCR2 was an obvious candidate due to its known role in neutrophil recruitment. Analysis of publicly available mouse leukocyte microarray data (www.immgen.org; gene name *IL8Rb*) confirmed that *Cxcr2* transcripts are firmly restricted to neutrophils. High expression of Gr1 is commonly used to identify blood neutrophils (30). The Gr1 Ab recognizes Ly6G and Ly6C: Ly6G is expressed by neutrophils, and they are the dominant $Ly6G^+$ cell type in mice (31). Ly6G is also expressed by neutrophil precursors in the bone marrow and polymorphonuclear MDSCs present in tumor-bearing mice (32). CXCR2 was highly expressed by all $Gr1^{hi}$ cells in blood of untreated mice, and also by most $Gr1^{hi}$ cells in bone marrow (Figure 1B); these cells in blood and bone marrow had the forward and side scatter properties of neutrophils, as expected (data not shown). $Gr1^{lo}$ blood cells (monocytes) were $CXCR2^-$ (Figure 1B).

Compared with adjacent normal skin, established DMBA/TPA-induced papillomas (harvested more than 2 weeks after the last TPA application) showed increased abundance of transcripts for at least 1 of the CXCR2 ligands, particularly *Cxcl1*, *Cxcl2*, and *Cxcl5* (Figure 1C), and a concomitant increase in levels of CXCL1, CXCL2, and CXCL5 protein (Figure 1D). Abs against CXCR2 ligands gave poor immunostaining of papillomas (data not shown), inconsistent with the levels of protein detected by ELISA (Figure 1D). Thus, to define the source of chemokines, RNA was prepared from stromal and tumor cells retrieved from papilloma sections by laser capture microdissection (LCM). Quantitative RT-PCR (Q-RT-PCR) did not detect any significant difference in expression of *Cxcl1* and *Cxcl2* between stroma and tumor, which indicates that they are made in both compartments, whereas *Cxcl5* was predominantly made by the stroma (Figure 1E). Thus, papillomas clearly had the potential to recruit $Gr1^{hi}$ blood cells through CXCR2. Moreover, CXCR2 was detected on most $CD11b^+Ly6G^+$ cells (Figure 1F) in disaggregated tumor samples (these cells were absent from adjacent normal tissue), albeit at lower levels than on blood and bone marrow $CD11b^+Ly6G^+$ cells from tumor-bearing mice (Figure 1G and data not shown). This was not unexpected in light of the high levels of tumor CXCL1, CXCL3, CXCL5, and/or CXCL7, since chronic chemokine exposure leads to CXCR2 internalization and degradation (33, 34). Weak CXCR2 immunoreactivity was found on the leukocyte infiltrate in sections of WT papillomas, but CXCR2 protein could not be detected by immunohistochemistry on any other cells within or around these tumors (data not shown). This was consistent with Q-RT-PCR data showing that *Cxcr2* transcripts were only increased approximately 3-fold above the very low levels found in noninflamed normal skin (Figure 1H). These transcripts were presumably primarily from the infiltrating $CXCR2^{lo}Ly6G^+$ cells, but low-level CXCR2 expression by other cells, including nonleukocytes, cannot be excluded.

*CXCR2 deficiency leads to MPO*$^+$ *cell paucity in TPA-inflamed skin and papillomas, reduced tumor microvessel density, and markedly suppressed papilloma formation*. To define indispensable roles for CXCR2 during tumor-promoting, and papilloma-driven, inflammation, we compared WT and *Cxcr2*$^{-/-}$ mice. We first examined the skin after single or multiple TPA applications. A single TPA application caused a time-dependent upregulation of transcripts for *Cxcl1*, *Cxcl2*, *Cxcl5*, and *Cxcl7* and an increase in *Cxcr2* mRNA in the skin (Figure 2A). Similarly, genes encoding CXCR2 ligands were induced by TPA administration to skin that had been chronically inflamed by repeated TPA application over a 2-week period (Figure 2B). Expression of genes encoding CXCR2 ligands peaked 12–24 hours after TPA application, coinciding with the time of highest *Cxcr2* expression. Compared with WT mice, *Cxcr2*$^{-/-}$ skin contained far fewer dermal and epidermal MPO$^+$ cells 6–24 hours after TPA application to naive or chronically inflamed skin (Figure 2C). MPO$^+$ cells detected in *Cxcr2*$^{-/-}$ skin were almost exclusively found in dermal blood vessels (Figure 2C). The MPO$^+$ cells recruited to the acutely inflamed skin of WT mice presumably originated from the blood $Gr1^{hi}$ ($Ly6G^+$) neutrophil pool, the predominant source of CXCR2-expressing cells in the circulation (Figure 1B). Indeed, the genes encoding neutrophilic granule protein (NGP) and CD177 (which, like CXCR2, are highly restricted to neutrophils; www.immgen.org) showed increased expression in inflamed skin relative to untreated skin (~2,500- and 200-fold, respectively; data not shown).

The neutrophil recruitment defect was accompanied by a reduced keratinocyte proliferative response in *Cxcr2*$^{-/-}$ skin 6–12 hours after application of TPA to naive or chronically inflamed skin, as assessed by Ki67 staining (Figure 2D). This was also seen 24 hours after TPA application to chronically, but not acutely, inflamed skin, but no differences were observed at 48 hours

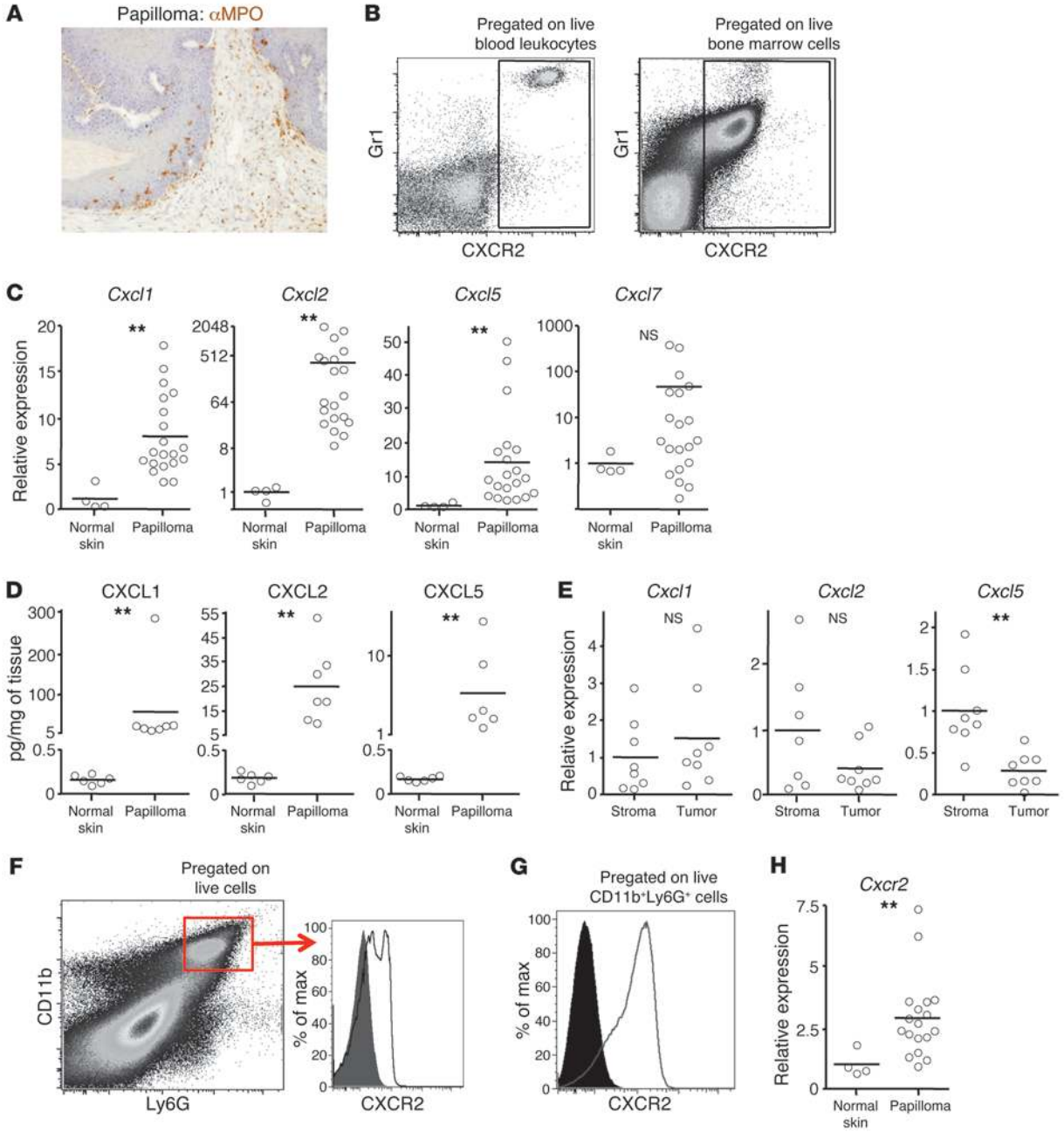


**Figure 1**

Expression of CXCR2 and its ligands in papillomas and blood. Papillomas were induced on WT Balb/c mice using DMBA/TPA. (**A**) Representative papilloma section immunostained with anti-MPO Ab (brown). Original magnification, ×200. (**B**) Live peripheral blood leukocytes (left) and bone marrow (right) immunostained with anti-Gr1 and anti-CXCR2 Ab and analyzed by flow cytometry. Gates defining $Gr1^+CXCR2^+$ cells (boxes) were set using anti-Gr1– and anti-CXCR2–immunostained *Cxcr2*$^{-/-}$ peripheral blood leukocytes and bone marrow and isotype control–stained WT cells. (**C**) Relative abundance of transcripts for CXCR2 ligands in WT papillomas (determined by Q-RT-PCR). Mean of normal adjacent skin is set to 1. (**D**) CXCL1, CXCL2, and CXCL5 protein in lysates of WT papillomas and resting normal skin, measured by ELISA. (**E**) Relative abundance of transcripts for *Cxcl1*, *Cxcl2*, and *Cxcl5* (determined by Q-RT-PCR) in stromal and tumor cells isolated from papillomas by LCM. Mean of stromal cells is set to 1. (**F**) Flow cytometry of a disaggregated papilloma (pregated for live cells) stained with anti-Ly6G and anti-CD11b Ab. Gate for $CD11b^+Ly6G^+$ cells (box) was defined using controls in which anti-Gr1 or anti-CD11b Ab had been replaced with an appropriate isotype control. Representative overlaid flow cytometry histogram plots of anti-CXCR2 (line) and isotype control (filled) immunostaining of $CD11b^+Ly6G^{hi}$ papilloma-associated cells are also shown. (**G**) As in **F**, but for $CD11b^+Ly6G^{hi}$ bone marrow cells. (**H**) As in **C**, but for *Cxcr2*. $^{**}P < 0.01$, Mann-Whitney test.

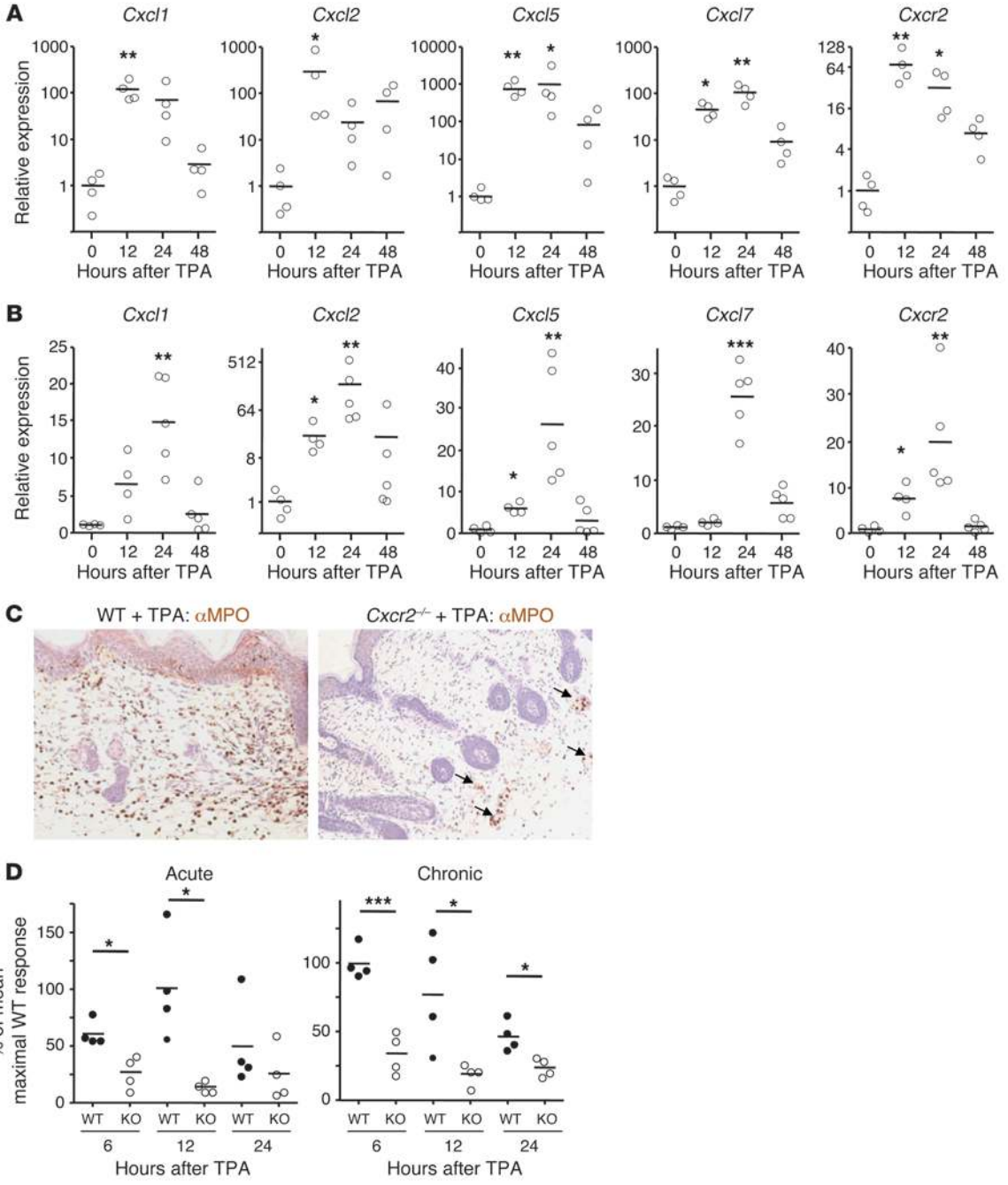


**Figure 2**

CXCR2 deficiency suppresses TPA-induced epidermal proliferation and neutrophil recruitment to inflamed skin. (**A** and **B**) Shaved back skin of WT Balb/c mice received TPA once (**A**), or 3 times per week for 2 weeks (**B**), and was harvested 12–48 hours after the final TPA treatment. Relative expression of *Cxcr2* and its ligands was determined by Q-RT-PCR; the mean of shaved, untreated skin (0 hours) is set to 1. *$P < 0.05$, **$P < 0.01$, ***$P < 0.001$ versus untreated, 1-way ANOVA with multiple comparison post-test. (**C**) Representative sections of anti-MPO–immunostained (brown) WT and *Cxcr2*$^{-/-}$ Balb/c back skin 12 hours after a single TPA treatment. Sections were counterstained with hematoxylin and visualized by light microscopy. MPO$^+$ cells in blood vessels are denoted by arrows. Original magnification, ×200. (**D**) Ki67$^+$ epidermal cells in WT and *Cxcr2*$^{-/-}$ (KO) Balb/c back skin 6, 12, and 24 hours either after a single TPA treatment (acute), or after the last of 6 TPA applications spanning 2 weeks (chronic). The mean of the maximal WT response in each data set is set to 100%. *$P < 0.05$, ***$P < 0.001$, 1-way ANOVA with multiple comparison post-test.

(Figure 2D and data not shown). 6–24 hours after a single cutaneous TPA application, when MPO$^+$ cells were at their peak, immunohistochemistry of inflamed WT skin (using *Cxcr2*$^{-/-}$ counterparts as negative controls) revealed the presence of CXCR2$^+$ cells among the inflammatory infiltrate (Supplemental Figure 1; supplemental material available online with this article; doi:10.1172/JCI61067DS1) that were absent from resting WT skin. No specific, reproducible anti-CXCR2 staining of epithelial or endothelial cells

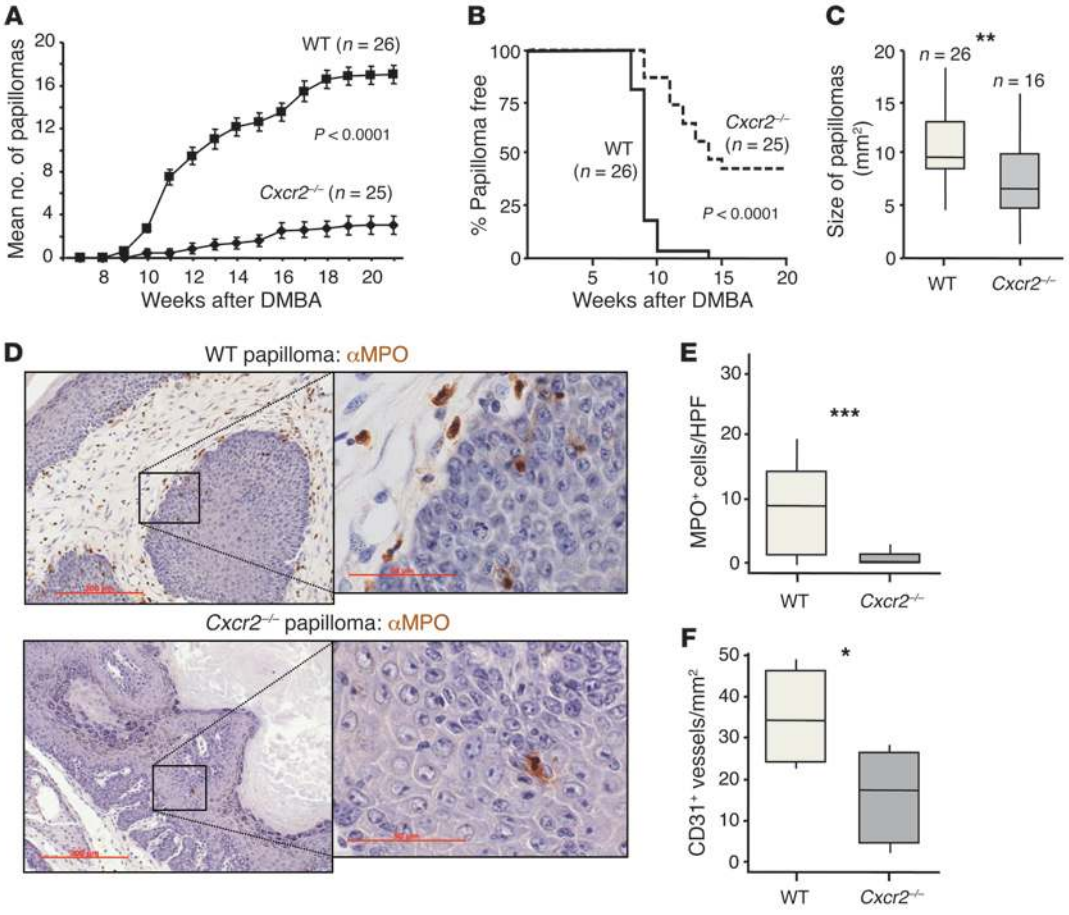


**Figure 3**

CXCR2 deficiency suppresses DMBA/TPA skin carcinogenesis. (**A**–**C**) WT and *Cxcr2*$^{-/-}$ Balb/c mice received DMBA once, followed 1 week later by 20 weeks of TPA treatment (3 times per week). Number of papillomas/mouse (**A**; mean ± SEM) and papilloma incidence (**B**) were recorded weekly. Tumors were measured at the end of the experiment (**C**). Data were analyzed by Mann-Whitney test (**A** at week 22 and **C**) and log-rank analysis with censoring (**B**). $^{**}P < 0.01$. (**D**) Representative sections of anti-MPO–immunostained (brown) WT and *Cxcr2*$^{-/-}$ Balb/c DMBA/TPA-induced papillomas. Sections were counterstained with hematoxylin and visualized by light microscopy. Boxed regions are shown at higher magnification in the insets. Scale bars: 200 μm; 50 μm (insets). (**E**) Average number of MPO$^+$ cells per high-powered field (HPF) of 6 papillomas taken from 4 or more mice of each genotype. $^{***}P < 0.001$, Mann-Whitney test. (**F**) Microvessel density in WT and *Cxcr2*$^{-/-}$ papillomas ($n$ = 5–6 per group). $^{*}P < 0.05$, Mann-Whitney test. Box and whisker plots show median (lines within boxes), interquartile range (bounds of boxes), and upper and lower range (whiskers).

was observed in WT skin (data not shown), although low levels of CXCR2 expression by nonleukocytes cannot be excluded.

Next, we assessed the overall effect of *Cxcr2* deficiency on papilloma development. We painted the dorsal skin of WT and *Cxcr2*$^{-/-}$ mice with a single dose of DMBA, followed by triweekly TPA treatments for 20 weeks. This robustly induced papillomas on WT mice, and, consistent with previous work (27), *Cxcr2*$^{-/-}$ mice were profoundly resistant to tumor induction. There was a substantial reduction in the average number of tumors formed (Figure 3A), and 40% of the *Cxcr2*$^{-/-}$ mice remained tumor free (Figure 3B). The papillomas that did develop on *Cxcr2*$^{-/-}$ mice were significantly smaller than those on WT animals (Figure 3C). MPO$^+$ cells associated with WT papillomas were nearly completely absent from *Cxcr2*$^{-/-}$ tumors (Figure 3, D and E). *Cxcr2* deficiency was also associated with a reduction in tumor microvessel density, with an average of approximately 50% fewer CD31$^+$ vessels/mm$^2$ in *Cxcr2*$^{-/-}$ than WT tumors (Figure 3F). The papillomas that developed on *Cxcr2*$^{-/-}$ mice were, however, no different from WT tumors in their expression of senescence markers, and BrdU incorporation and expression of markers of DNA repair, apoptosis, or proliferation were not noticeably different between WT and *Cxcr2*$^{-/-}$ tumors (Supplemental Figure 2, A and B). Thus, CXCR2 was critical for the recruitment of MPO$^+$ cells into inflamed skin and papillomas; enhanced keratinocyte proliferation during cutaneous inflammation and microvessel density in skin tumors; and played a central protumorigenic role in DMBA/TPA-induced papillomagenesis.

*CXCR2 deletion suppresses colitis-associated tumorigenesis.* To explore the general relevance of CXCR2 to inflammation-associated cancer, we next examined whether *Cxcr2* deficiency influences colitis-associated cancer. In this protocol, mice were given a single i.p. injection of the mutagen azoxymethane (AOM) at 12.5 mg/kg followed by several 5-day periods of feeding 2% dextran sodium sulfate (DSS) in the drinking water, interspersed with periods on normal water (Supplemental Figure 3).

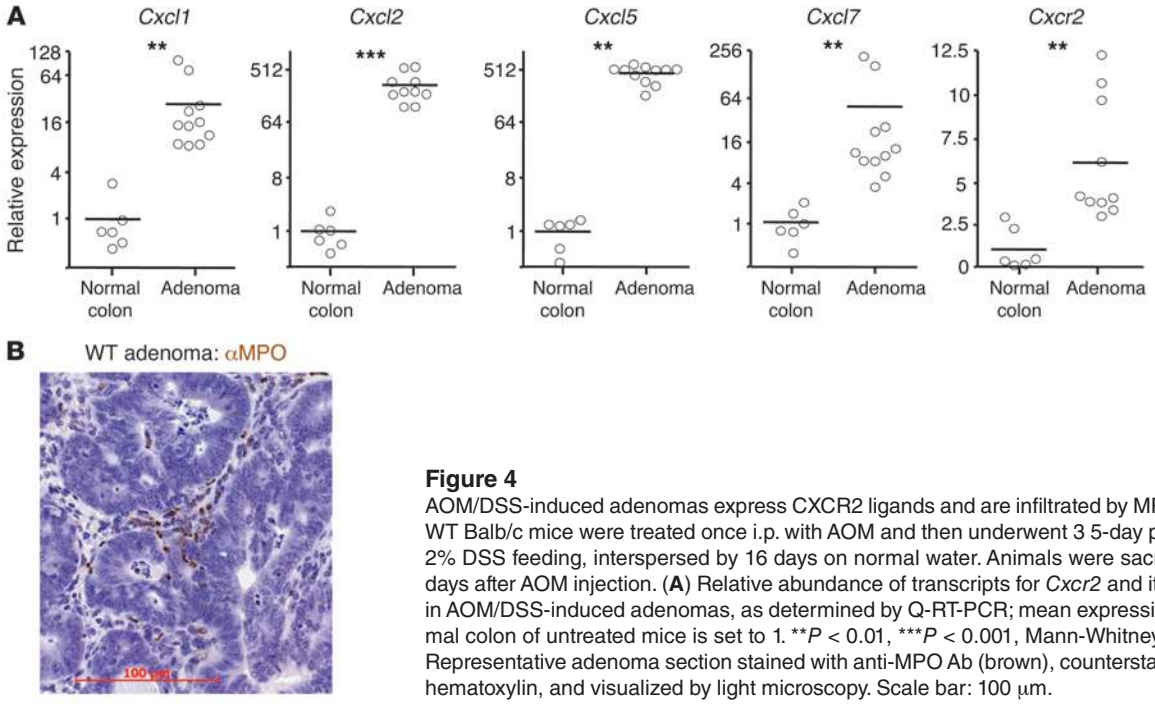


**Figure 4**
AOM/DSS-induced adenomas express CXCR2 ligands and are infiltrated by MPO$^+$ cells. WT Balb/c mice were treated once i.p. with AOM and then underwent 3 5-day periods of 2% DSS feeding, interspersed by 16 days on normal water. Animals were sacrificed 70 days after AOM injection. (**A**) Relative abundance of transcripts for *Cxcr2* and its ligands in AOM/DSS-induced adenomas, as determined by Q-RT-PCR; mean expression in normal colon of untreated mice is set to 1. $^{**}P < 0.01$, $^{***}P < 0.001$, Mann-Whitney test. (**B**) Representative adenoma section stained with anti-MPO Ab (brown), counterstained with hematoxylin, and visualized by light microscopy. Scale bar: 100 μm.

As in the DMBA/TPA-induced skin papillomas, *Cxcl1*, *Cxcl2*, *Cxcl5*, and *Cxcl7* were all substantially elevated in all AOM/DSS-induced colonic polyps from WT mice, and there was a small increase in *Cxcr2* expression (Figure 4A). These adenomas were harvested 2–3 weeks after the final DSS treatment, and were thus constitutively producing these chemokines in the absence of exogenous inflammatory stimuli. MPO$^+$ cells were present in the stromal compartment directly adjacent to the neoplastic epithelial cells in all WT tumors analyzed (Figure 4B). Thus, AOM/DSS-induced adenomas expressed the chemokines capable of recruiting blood Ly6G$^+$ cells and contained populations of infiltrating MPO$^+$ cells.

2% DSS drives colitis-associated tumorigenesis, but only mild clinical symptoms of colitis develop in WT mice during the 2% DSS feeding periods. Higher doses (3.5%–5% DSS) are required to substantially disrupt colonic integrity. This leads to infiltration of the lamina propria by inflammatory cells and clinical symptoms of colitis. CXCR2 inhibition has been reported to protect Balb/c mice from the effects of 4%–5% DSS (35, 36); consistent with this, CXCR2 deficiency provided effective protection from the clinical and histopathological symptoms of colitis induced by 3.5% DSS (Supplemental Figure 4A). With progressive DSS-induced damage, WT colons showed strong upregulation of expression of CXCR2 chemokine ligands, concomitant with increased CXCR2 expression (Supplemental Figure 4B). This was accompanied by MPO$^+$ cell infiltration of the WT lamina propria that was markedly reduced in *Cxcr2*$^{-/-}$ mice (Supplemental Figure 4C). No obvious clinical symptoms developed in WT or *Cxcr2*$^{-/-}$ mice during feeding with 2% DSS (data not shown). There were, however, increases in chemokine mRNA levels in WT colons, as assessed by Q-RT-PCR, with *Cxcl1*, *Cxcl2*, and *Cxcl5* showing statistically significant upregulation after 5 days of DSS exposure (Figure 5A). Moreover, localized histological changes were present in WT colons after 5 days of 2% DSS feeding, as well as at day 7 (i.e., 2 days after reverting to DSS-free water; Figure 5B and data not shown). These inflamed areas contained substantial numbers of MPO$^+$ cells, localized primarily near the colonic crypts (Figure 5B), and on day 7 showed extensive epithelial proliferation (assessed by BrdU incorporation; Figure 5C). In contrast, the structure of *Cxcr2*$^{-/-}$ colons was unaffected by exposure to 2% DSS; the lamina propria contained few extravascular MPO$^+$ cells; and intestinal epithelial cells incorporated BrdU in a manner comparable to that of mice that had not received DSS (Figure 5, B and C). The MPO$^+$ cells recruited to the acutely inflamed colons of WT mice were likely to be derived from the circulating Ly6G$^+$ neutrophil pool, the predominant CXCR2$^+$ cell type in the blood (Figure 1B). Thus, CXCR2 deficiency substantially altered the colonic response to low and high doses of DSS.

Next, we considered the overall effect of *Cxcr2* deletion on adenoma development. *Cxcr2*$^{-/-}$ mice were highly resistant to the induction of adenomas by AOM/DSS treatment, developing far fewer tumors that were significantly smaller than those present in WT animals, leading to an approximately 90% reduction in tumor burden (Figure 6A). MPO$^+$ cells present in the stromal compartment of WT tumors were virtually absent from *Cxcr2*$^{-/-}$ adenomas (Figure 6B), and there was a substantial reduction in microvessel density in *Cxcr2*$^{-/-}$ tumors (Figure 6C). Thus, as in DMBA/TPA-induced skin tumorigenesis, CXCR2 played a strong protumorigenic role in colitis-associated cancer.

*Spontaneous mouse tumors express genes encoding CXCR2 ligands and contain MPO$^+$ cells, and CXCR2 ligands are a prominent part of the Apc$^{Min/+}$ adenoma secretome.* CXCR2-mediated leukocyte recruitment, a key component of TPA- and DSS-driven inflammation, likely makes a substantial contribution to the strong protumorigenic role of CXCR2 in these tissues. Nonetheless, in both models, it is also likely that CXCR2 contributes to the tumor-driven inflammatory response, because long after treatment with exogenous inflammatory stimuli was discontinued, all established tumors had evolved to constitutively express high levels of CXCR2 ligands and contained CXCR2-dependent MPO$^+$ cells. Most

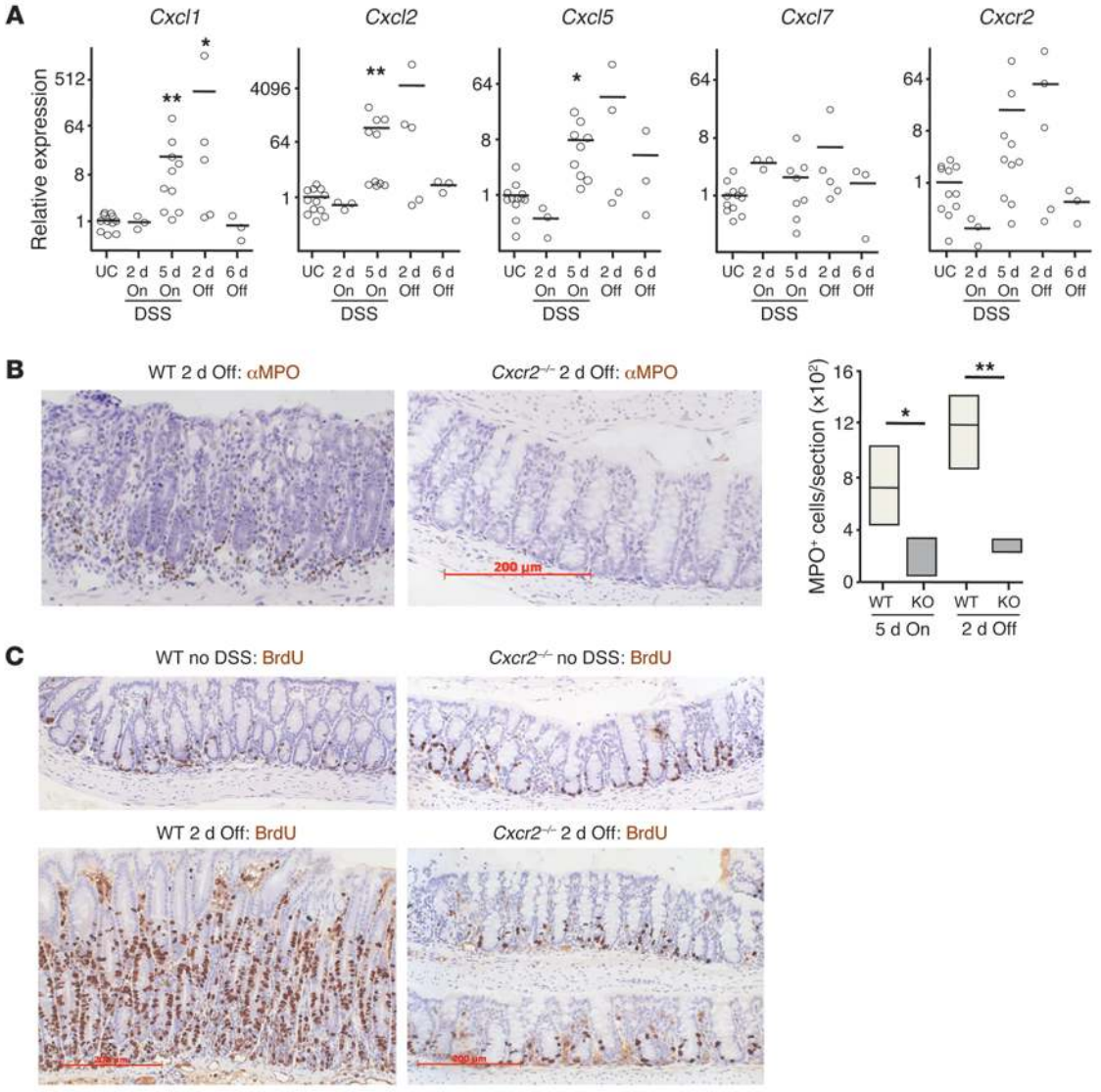


**Figure 5**

*Cxcr2* deficiency protects against intestinal inflammation induced by 2% DSS. WT and *Cxcr2*$^{-/-}$ mice were fed 2% DSS for 5 days and then normal water for a further 6 days. (**A**) Relative expression of *Cxcr2* and its ligands in WT Balb/c colon during 2% DSS feeding, as determined by Q-RT-PCR; mean expression in colon of untreated control mice (UC) is set to 1. On refers to duration of 2% DSS feeding; Off refers to duration of return to normal water. **P* < 0.05, ***P* < 0.01 versus untreated control, 1-way ANOVA with multiple comparison post-test. (**B** and **C**) Representative sections of colons from WT and *Cxcr2*$^{-/-}$ Balb/c mice immunostained with anti-MPO (**B**) or anti-BrdU (**C**) Ab (brown), either 2 days after returning to normal water or in the absence of DSS exposure. Mice were injected i.p. with BrdU 2 hours before harvest. Sections were counterstained with hematoxylin and visualized by light microscopy. The number of MPO$^+$ cells per section of WT and *Cxcr2*$^{-/-}$ (KO) colons after 5 days of 2% DSS feeding and 2 days after return to normal water ($n = 4$ per group) is also shown in **B**. **P* < 0.05, ***P* < 0.01, Mann-Whitney test. Scale bars: 200 μm (**B** and **C**). Box and whisker plots show median (lines within boxes), interquartile range (bounds of boxes), and upper and lower range (whiskers).

human tumors do not arise in the context of preexisting chronic tissue-wide inflammatory disease, and therefore it was important to examine the role of CXCR2 in spontaneous malignancy in the absence of experimentally induced chronic tissue inflammation.

For this purpose, we used 3 spontaneous mouse models of cancer: the *Apc*$^{Min/+}$ model of benign intestinal adenomas (37), the *AhCreER;Apc*$^{fl/+}$*;Pten*$^{fl/fl}$ model of invasive intestinal adenocarcinoma (38), and the *K14CreER;KRas*$^{G12D/+}$ model of spontaneous oral papilloma formation (39, 40). Like the inflammation-driven tumors, there was a substantial increase in mRNA expression of at least 1, and often all 4, of the genes encoding CXCR2 ligands in all the tumors analyzed from these models (Figure 7, A and B, and Supplemental Figure 5A). In the *AhCreER;Apc*$^{fl/+}$*;Pten*$^{fl/fl}$ model, invasive tumors typically had higher expression of genes encoding CXCR2 ligands than noninvasive tumors, but *Cxcl2* was expressed, on average, approximately 100-fold higher than control in both invasive and noninvasive tumors (Figure 7B). In all *Apc*$^{Min/+}$ tumor lysates we analyzed, protein for at least 1 of the chemokines CXCL1, CXCL2, or CXCL5 was readily detected, but all were barely detectable in lysates of normal intestine (Figure 7C).

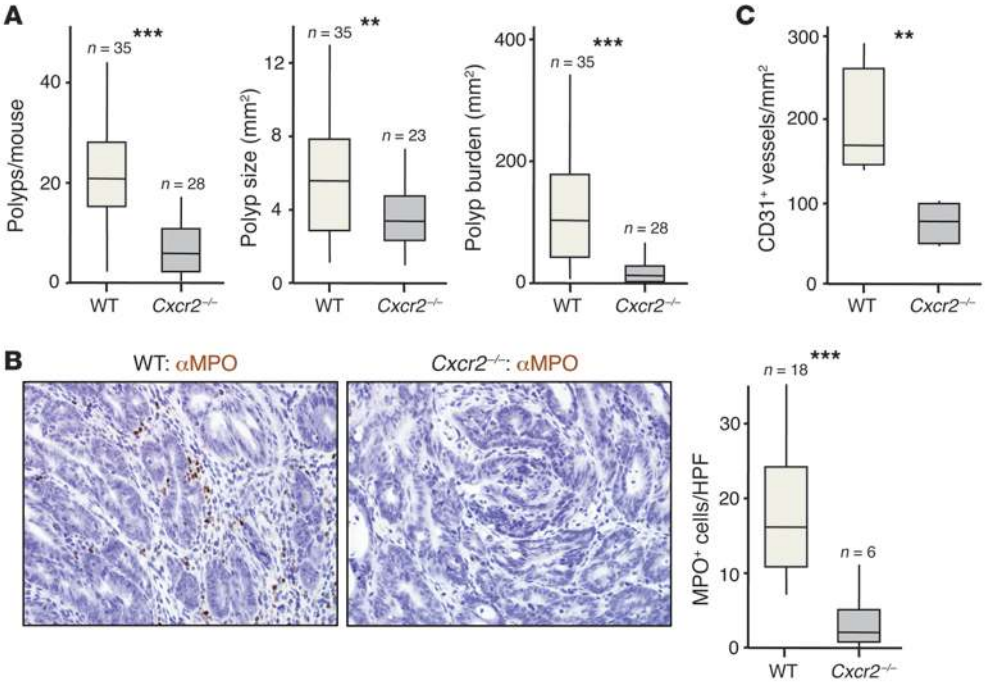


**Figure 6**

*Cxcr2* deficiency suppresses AOM/DSS-induced adenoma formation. WT and *Cxcr2*$^{-/-}$ mice were treated once i.p. with AOM and then underwent 3 5-day periods of 2% DSS feeding, interspersed by 16 days on normal water. Animals were sacrificed 70 days after AOM injection. (**A**) Number of colonic polyps per mouse, polyp size, and overall tumor burden per mouse (*n* as indicated). (**B**) Representative sections of AOM/DSS-induced adenomas from WT and *Cxcr2*$^{-/-}$ mice immunostained with anti-MPO (brown), counterstained with hematoxylin, and visualized by light microscopy. Number of MPO$^+$ cells per high-powered field in sections of WT and *Cxcr2*$^{-/-}$ adenomas (*n* as indicated) is also shown. (**C**) Microvessel density in WT and *Cxcr2*$^{-/-}$ adenomas ($n = 5–6$ per group). $^{**}P < 0.01$, $^{***}P < 0.001$, Mann-Whitney test. Box and whisker plots show median (lines within boxes), interquartile range (bounds of boxes), and upper and lower range (whiskers).

Using cytokine Ab arrays and ELISAs, we next analyzed conditioned media from stroma-free primary *Apc*$^{Min/+}$ adenomas and crypt cultures established from WT mice. This revealed CXCL1, CXCL2, CXCL5, and CXCL7 were abundant components of the *Apc*$^{Min/+}$ tumor secretome (Figure 7D and Supplemental Figure 6). Q-RT-PCR confirmed increased expression of these genes by *Apc*$^{Min/+}$ adenoma cultures (data not shown). In fact, of the approximately 100 cytokines and secreted factors analyzed on the arrays, CXCL1, CXCL2, CXCL5, and CXCL7 were among the top 6 proteins most differentially expressed between cultured primary *Apc*$^{Min/+}$ adenomas and WT crypt cultures; notably, none of the other 10 or so inflammatory chemokines that could be detected using the arrays were substantially upregulated in *Apc*$^{Min/+}$ adenoma cultures (data not shown). Moreover, transcriptomics failed to identify any inflammatory chemokines that were consistently elevated in RNA samples prepared from *Apc*$^{Min/+}$ tumors immediately after dissection from the intestine, compared with samples from tumor-free intestine (data not shown). Thus, *Apc*$^{Min/+}$ tumor cells abundantly expressed at least 1, and often more, of the CXCR2 chemokine ligands, and these chemokines formed a specific and prominent part of the tumor-associated secretome.

Relative to normal tissue, *Cxcr2* was also upregulated in tumors from the 3 models (Figure 7, A and B, and Supplemental Figure 5A). Tumor sections immunostained with anti-CXCR2 Ab failed to reveal any reproducible evidence of CXCR2 expression by epithelial, endothelial, or tumor cells, although low-level expression of CXCR2 by these cells cannot be excluded. However, weak anti-CXCR2 immunoreactivity was observed on leukocytes in the stromal compartment (Figure 8A). The large majority of the tumors analyzed contained MPO$^+$ cells, usually located in the stroma directly underlying the tumor cells, and sometimes among the tumor cells (Figure 8B and Supplemental Figure 5B). These cells were rare outside of blood vessels in normal adjacent tissue (data not shown). In *Apc*$^{Min/+}$ and *AhCreER;Apc*$^{fl/+}$*;Pten*$^{fl/fl}$ mice, even small lesions contained substantial populations of MPO$^+$ cells, and in invasive *AhCreER;Apc*$^{fl/+}$*;Pten*$^{fl/fl}$ tumors, MPO$^+$ cells were particularly noticeable at the invasive front (Figure 8B).

To confirm the presence of similar cell populations within the stroma of human intestinal adenomas, we stained human adenoma sections with Ab against MPO. Indeed, 12 of 15 human colonic adenomas that we screened contained MPO$^+$ cells, at varying densities, within the tumor stroma and occasionally within the neoplastic epithelium (Supplemental Figure 7). Thus, MPO$^+$ cell infiltration was a common feature of human colonic adenomas, as in the mouse models.

*CXCR2 inhibition suppresses spontaneous development of benign tumors.* We next investigated whether CXCR2 contributed to spontaneous tumorigenesis in *Apc*$^{Min/+}$ mice. Due to genetic modifiers strongly modulating tumorigenesis in this strain, only mice with purebred C57BL/6J background can be reliably used (41). Because *Cxcr2*$^{-/-}$ mice were on a Balb/c background, to avoid extensive backcrossing, we instead chose to use pepducin inhibitors of CXCR2 (24). Kaneider and colleagues developed pepducins that specifically target CXCR1 and CXCR2 and used

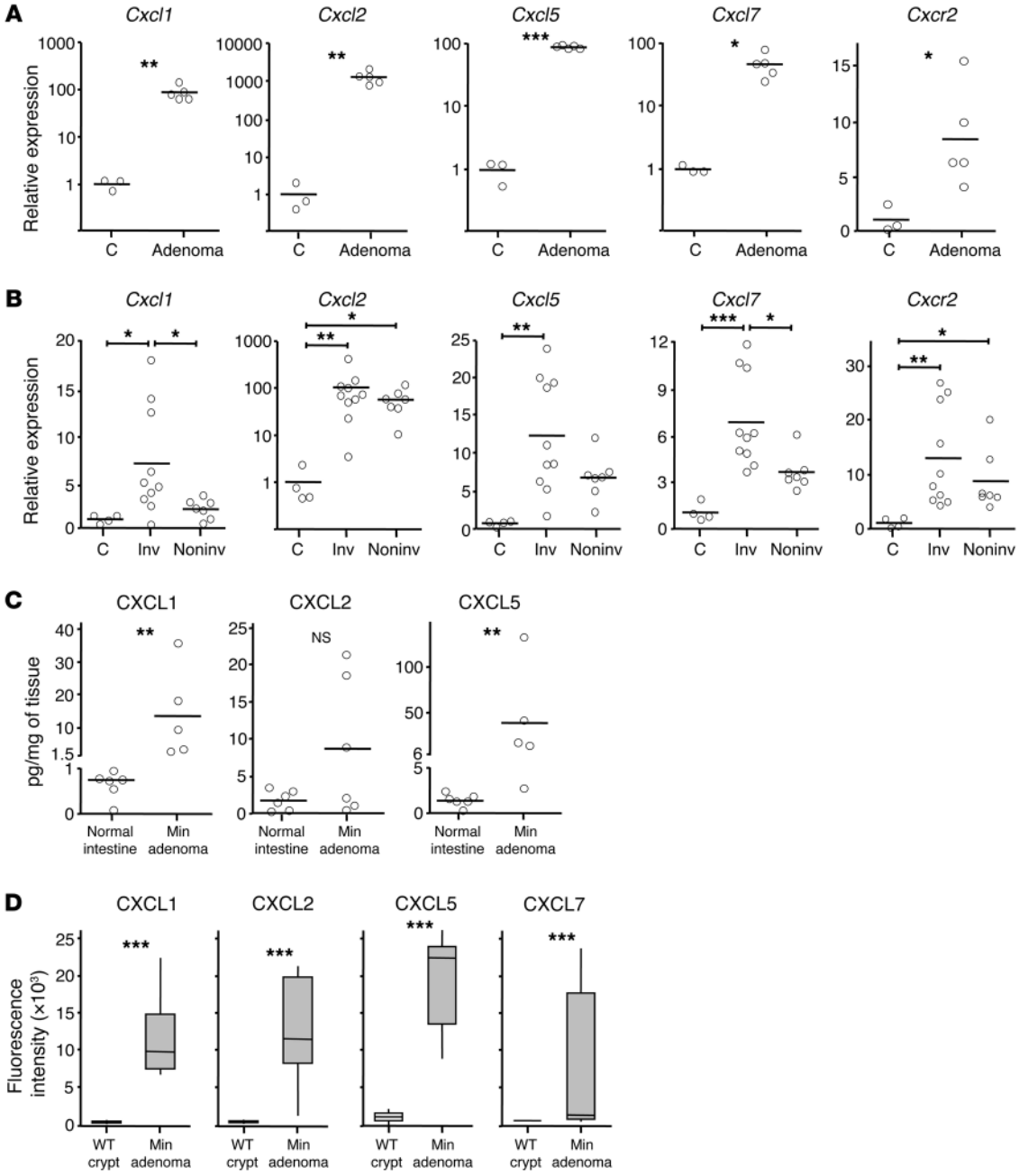


**Figure 7**

Genes encoding CXCR2 ligands are highly expressed by spontaneous intestinal tumors and form part of the secretome of *Apc*$^{Min/+}$ adenomas. (**A** and **B**) Relative mRNA expression of *Cxcr2* and its ligands in tumors from *Apc*$^{Min/+}$ (**A**) and *AhCreER;Apc*$^{fl/+}$*;Pten*$^{fl/fl}$ (**B**) mice. Tumors from *AhCreER;Apc*$^{fl/+}$*;Pten*$^{fl/fl}$ mice were harvested approximately 50 days after cre activation (4 i.p. injections of cre inducers) and categorized as invasive (Inv) or noninvasive based on examination of intestinal tissue and confirmed by microscopic examination of H&E-stained sections. Mean expression in adjacent normal tissue (C) is set to 1. (**C**) CXCL1, CXCL2, and CXCL5 protein in lysates of *Apc*$^{Min/+}$ adenomas and resting normal intestine from C57BL/6 mice, measured by ELISA. (**D**) Mouse cytokine antibody arrays were exposed to conditioned media from cultures of WT intestinal crypts or *Apc*$^{Min/+}$ adenomas, and fluorescence intensity on anti-CXCL1, -CXCL2, -CXCL5, and -CXCL7 Ab was read on a microarray scanner ($n = 5$ per group). $^{*}P < 0.05$, $^{**}P < 0.01$, $^{***}P < 0.001$, Mann-Whitney test (**A**, **C**, and **D**) or 1-way ANOVA with multiple comparison post-test (**B**). Box and whisker plots show median (lines within boxes), interquartile range (bounds of boxes), and upper and lower range (whiskers).

them to block sepsis in mice (24). We treated *Apc*$^{Min/+}$ mice daily from 35 days old with pepducin or a nontargeting pepducin control, harvesting intestines when the animals were 85 days old. Control *Apc*$^{Min/+}$ mice developed large numbers of intestinal adenomas, as expected, but this was reduced by treatment with the CXCR1/2-blocking pepducin (Figure 9A). Those tumors that did develop in animals treated with CXCR1/2 pepducin contained few MPO$^{+}$ cells, unlike controls (Figure 9, B and C).

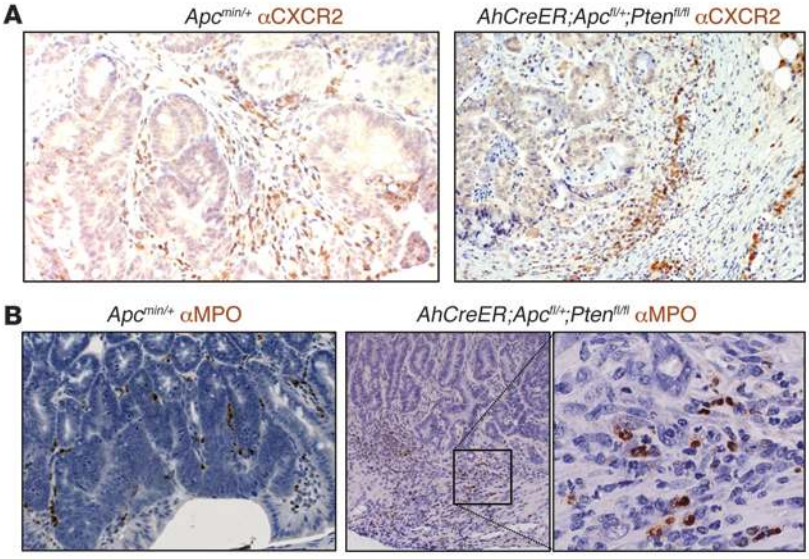


**Figure 8**
CXCR2$^+$ and MPO$^+$ cells infiltrate spontaneous intestinal tumors. Representative adenomas from *Apc$^{min/+}$* and *AhCreER;Apc$^{fl/+}$;Pten$^{fl/fl}$* mice immunostained (brown) with Ab against CXCR2 (**A**) or MPO (**B**), counterstained with hematoxylin, and visualized by light microscopy. Tumors from *AhCreER;Apc$^{fl/+}$;Pten$^{fl/fl}$* tumors were harvested approximately 50 days after cre activation (4 i.p. injections of cre inducers). The boxed region in **B** is shown at higher magnification in the inset. Original magnification, ×200; ×400 (higher-magnification view).

Microvessel density, however, was unaffected by CXCR1/2 pepducin treatment (Figure 9D).

In the *K14CreER;KRas$^{G12D/+}$* model, sporadic cre activity during development drives the rapid emergence of oral papillomas shortly after weaning (40), and these animals often have to be euthanized before they can breed. As a consequence, it proved difficult to generate cohorts of *K14CreER;KRas$^{G12D/+}$* mice in which both *Cxcr2* alleles were deleted. Nonetheless, we found that haploinsufficiency for *Cxcr2* was able to significantly slow tumorigenesis in this short latency oral papilloma model (Supplemental Figure 5C).

*CXCR2 deficiency suppresses spontaneous development of intestinal adenocarcinomas*. Since CXCR2 inhibition or deficiency strongly suppressed inflammation-driven and spontaneous benign tumor formation, we next examined whether it had any effect on intestinal adenocarcinoma formation in *AhCreER;Apc$^{fl/+}$;Pten$^{fl/fl}$* mice (38). In this model, cre recombinase induction in the intestine, by treatment with β-napthoflavone and tamoxifen, is used to delete 1 copy of *Apc* and both copies of *Pten* and leads to the rapid development of intestinal adenocarcinomas after the sporadic loss of the remaining *Apc* allele (38). First, we examined the effect of CXCR2 deficiency on short-term responses to cre induction (i.p. injection on 4 consecutive days with β-napthoflavone and tamoxifen) using *AhCreER;Apc$^{fl/fl}$;Pten$^{fl/fl}$;Cxcr2$^{+/+}$* and *AhCreER;Apc$^{fl/fl}$;Pten$^{fl/fl}$;Cxcr2$^{-/-}$* mice. Regardless of *Cxcr2* genotype, cre induction led to epithelial hyperproliferation, nuclear β-catenin, and increased expression of p-AKT and cleaved caspase 3 (Supplemental Figure 8). Moreover, although a few MPO$^+$ cells were present in the lamina propria 6 days after cre induction, their presence was unaffected by *Cxcr2* genotype (Supplemental Figure 8). In addition, in contrast to the tumors that developed in *AhCreER;Apc$^{fl/+}$;Pten$^{fl/fl}$* mice (Figure 7B), genes encoding CXCR2 ligands were not upregulated after cre-induced deletion of *Pten* and/or *Apc*: in fact, some were significantly downregulated after cre induction (Supplemental Figure 9). Thus, *Cxcr2* deficiency did not noticeably affect early responses to cre induction in *AhCreER;Apc$^{fl/fl}$;Pten$^{fl/fl}$* mice.

Next, we treated cohorts of *AhCreER;Apc$^{fl/+}$;Pten$^{fl/fl}$;Cxcr2$^{+/+}$* and *AhCreER;Apc$^{fl/+}$;Pten$^{fl/fl}$;Cxcr2$^{-/-}$* mice on 4 consecutive days i.p. with β-napthoflavone and tamoxifen and harvested 50 days later.

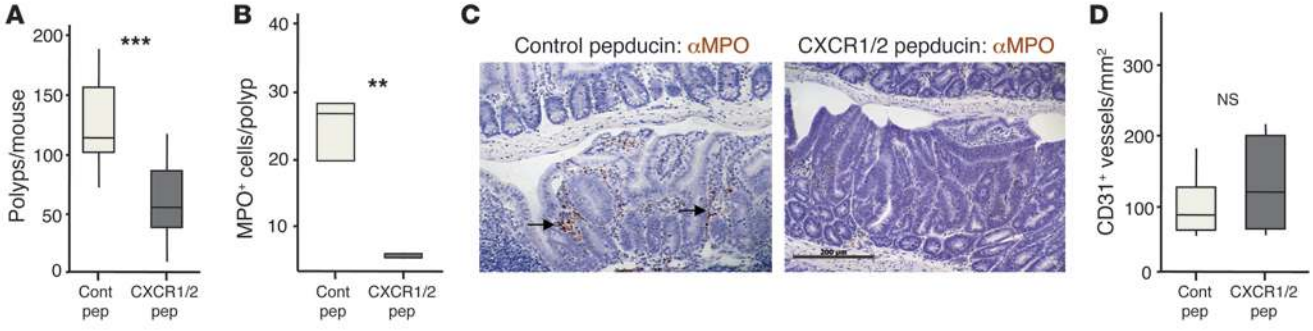


**Figure 9**
CXCR2 inhibition suppresses spontaneous formation of benign cancers in *Apc$^{Min/+}$* mice. *Apc$^{Min/+}$* mice were treated with control or CXCR1/2 pepducin from 5 weeks of age and sacrificed 50 days later. (**A**) Number of polyps per mouse. (**B**) Number of MPO$^+$ cells per polyp section. (**C**) Representative sections of adenomas from pepducin-treated *Apc$^{min/+}$* mice were immunostained with Ab against MPO (brown), counterstained with hematoxylin, and visualized by light microscopy. Clusters of MPO$^+$ cells are indicated by arrows. (**D**) Microvessel density of adenomas from pepducin-treated *Apc$^{Min/+}$* mice ($n$ = 5–6 mice per group). $^{**}P < 0.01$, $^{***}P < 0.001$, Mann-Whitney test. Box and whisker plots show median (lines within boxes), interquartile range (bounds of boxes), and upper and lower range (whiskers).

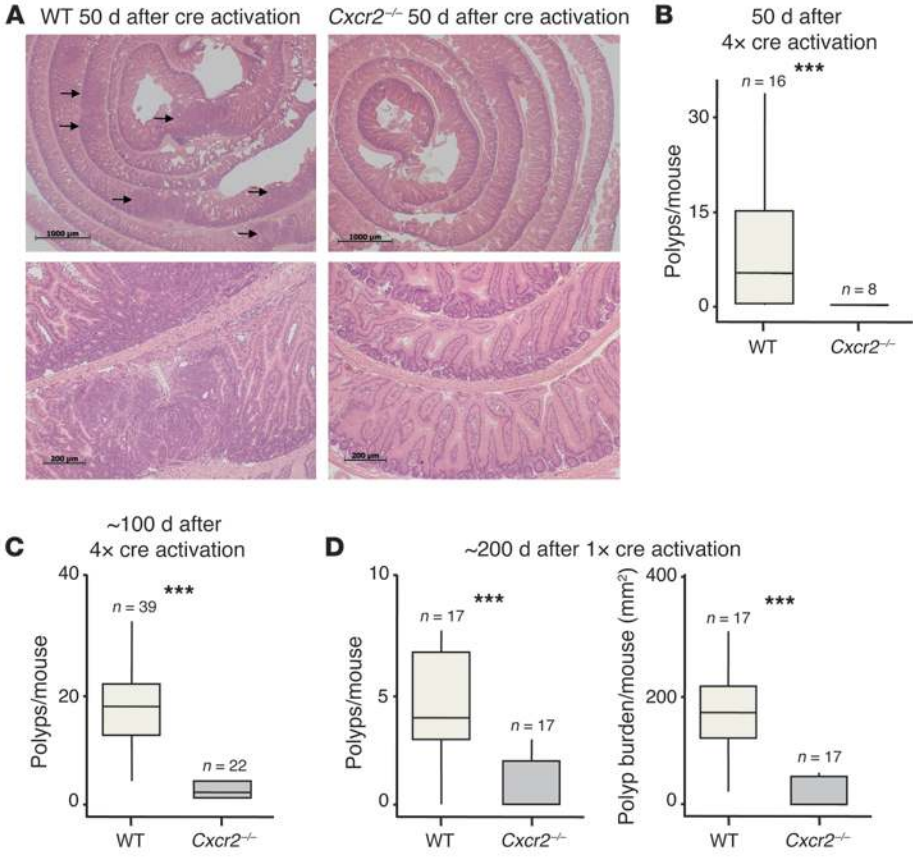


**Figure 10**
*Cxcr2* deficiency suppresses intestinal adenocarcinoma formation. Cohorts of *AhCreER;Apc*$^{fl/+}$*;Pten*$^{fl/fl}$*;Cxcr2*$^{+/+}$ (WT) and *AhCreER;Apc*$^{fl/+}$*;Pten*$^{fl/fl}$*;Cxcr2*$^{-/-}$ (*Cxcr2*$^{-/-}$) mice were injected i.p. on 4 consecutive days (**A**–**C**) or once (**D**) with cre inducers (tamoxifen and β-napthoflavone). Mice were sacrificed after 50 (**A** and **B**), 100 (**C**), or 200 (**D**) days. (**A**) Representative H&E-stained colonic rolls taken at low (×2.5; top) and high (×20; bottom) magnification. Arrows denote adenomas. Scale bars: 1,000 μm (top); 200 μm (bottom). (**B** and **C**) Number of polyps per mouse (*n* as indicated). (**D**) Polyps and tumor burden per mouse (*n* as indicated). The median value for *AhCreER;Apc*$^{fl/+}$*;Pten*$^{fl/fl}$*;Cxcr2*$^{-/-}$ mice is 0. ***$P < 0.001$, Mann-Whitney test. Box and whisker plots show median (lines within boxes), interquartile range (bounds of boxes), and upper and lower range (whiskers).

This induced multiple tumors in *AhCreER;Apc*$^{fl/+}$*;Pten*$^{fl/fl}$*;Cxcr2*$^{+/+}$ mice, as expected (38). However, intestinal tumors could not be found in any of the *Cxcr2*$^{-/-}$ mice at this time point, either by gross inspection of the intestine or by examination of H&E-stained tissue sections (Figure 10, A and B). When the period after cre induction was extended to 100 days (or the point of euthanasia), *Cxcr2*$^{-/-}$ mice again showed a substantial reduction in tumor burden (Figure 10C). Only 1 of the 16 tumor-bearing *Cxcr2*$^{-/-}$ animals had any evidence of invasive adenocarcinoma, in contrast to 16 of the 22 WT animals examined ($P = 0.001$, $\chi^2$ test). The rare tumors that did develop in the absence of *Cxcr2* contained far fewer MPO$^+$ cells than did *AhCreER;Apc*$^{fl/+}$*;Pten*$^{fl/fl}$*;Cxcr2*$^{+/+}$ tumors (data not shown). A reliable comparison of microvessel density was not possible due to the low number of tumors present in *AhCreER;Apc*$^{fl/+}$*;Pten*$^{fl/fl}$*;Cxcr2*$^{-/-}$ mice. Finally, we treated mice with a single injection of cre inducers, a procedure that slows tumor development and reduces tumor multiplicity. Animals were analyzed 200 days after cre induction, although some of the mice became moribund before this, and thus were culled and analyzed earlier. Again, *Cxcr2* deficiency provided marked protection against the development of intestinal tumors (Figure 10D). Thus, CXCR2 proved a critical factor in the development of intestinal tumors in *AhCreER;Apc*$^{fl/+}$*;Pten*$^{fl/fl}$ mice after cre induction, to an even greater extent than in the AOM/DSS model.

*Long-term Ly6G$^+$ cell depletion suppresses intestinal tumorigenesis.* The data above revealed the importance of CXCR2 in inflammation-driven and spontaneous tumorigenesis in the skin and intestine. Because CXCR2 was predominantly expressed by Ly6G$^+$ (Gr1$^{hi}$) leukocytes, we anticipated that their CXCR2-dependent recruitment into inflamed tissues and tumors was playing a major protumorigenic role. However, *Cxcr2*$^{-/-}$ mice consistently had lower microvessel density, and although we were unable to detect CXCR2 on endothelial cells by immunohistochemistry, its absence from these cells might contribute to the reduction in tumor burden seen in *Cxcr2*$^{-/-}$ mice. We were therefore interested in specifically assessing the contribution of Ly6G$^+$ (Gr1$^{hi}$) leukocytes to tumorigenesis in our models. The 1A8 Ab recognizes Ly6G and is often used to deplete Ly6G$^+$ cells in vivo. Here, compared with control animals injected with equivalent quantities of isotype-matched Ab (2A3), a single injection of 1A8 substantially reduced the numbers of circulating neutrophils (identified using both an ADVIA 2120 Hematology System and flow cytometry after immunostaining for CXCR2 and Gr1), and this could be maintained for at least 3 weeks with triweekly 1A8 injections (Supplemental Figure 10).

To explore the effect of long-term Ly6G$^+$ cell depletion on tumorigenesis, WT mice undergoing AOM/DSS treatment were injected 3 times per week with 1A8 or isotype control (2A3) from the start of the first DSS feed, and harvested after 2 cycles of DSS (Figure 11, A–C). Compared with controls, 1A8-treated mice had approximately 70% fewer polyps; those polyps that did develop were, on average, smaller; and there was an overall reduction in tumor burden of 80%–90% (Figure 11A). At the time of sacrifice, there were much fewer blood neutrophils in mice treated with 1A8 than with isotype control (Figure 11B). MPO$^+$ cells were absent from the tumors that did develop in 1A8-treated mice (data not shown), which suggests, as expected, that Ly6G$^+$ leukocytes recruited from the blood give rise to MPO$^+$ cells in the tumor. Ly6G$^+$ cell depletion and *Cxcr2* deficiency suppressed

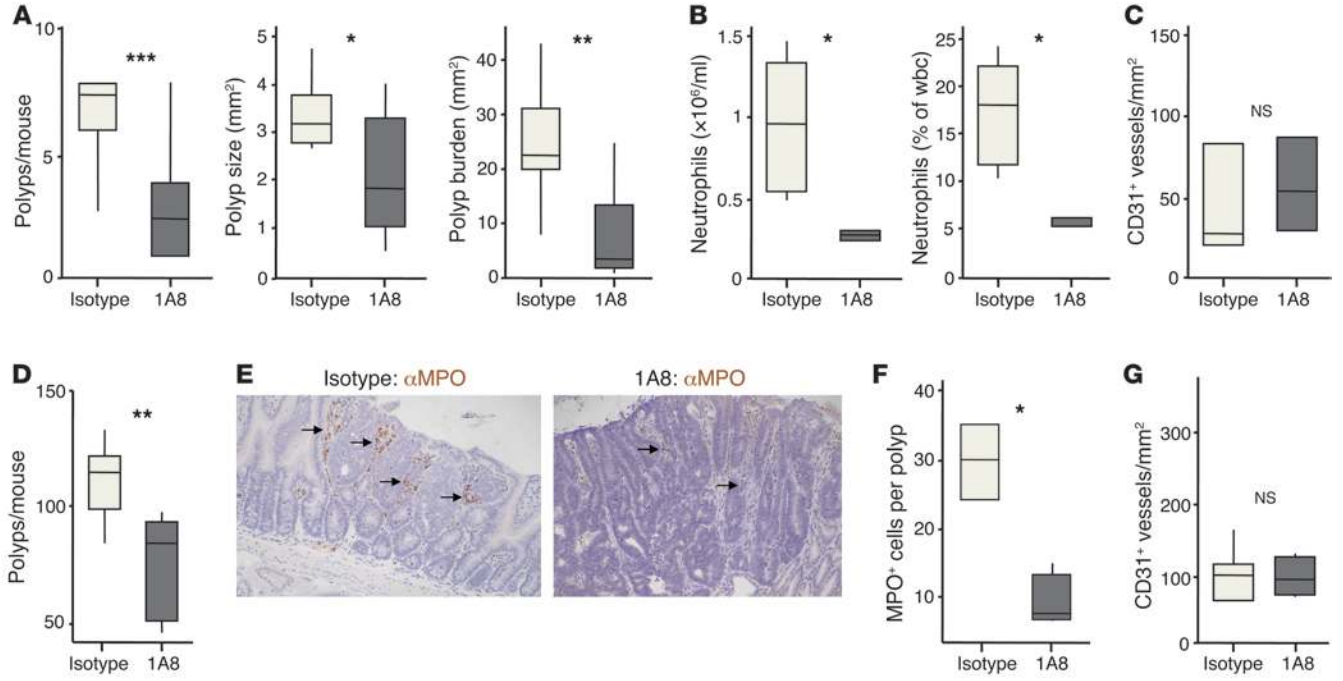


**Figure 11**

Ly6G⁺ cell depletion suppresses AOM/DSS-induced and spontaneous intestinal tumorigenesis. (**A**–**C**) WT Balb/c mice were injected with AOM and then underwent 2 5-day periods of 2% DSS feeding, interspersed by 16 days on normal water. From the start of the first DSS feed, groups of 10 mice were treated 3 times per week with either 1A8 (anti-Ly6G) or isotype control (2A3) Ab. (**A**) Number of colonic polyps per mouse, polyp size, and overall tumor burden per mouse. (**B**) Blood neutrophil counts, expressed as total and percentage, on the day of sacrifice ($n$ = 5 [isotype]; 4 [1A8]). (**C**) Microvessel density in adenomas ($n$ = 3 per group). (**D**–**G**) $Apc^{Min/+}$ mice were treated 3 times per week with either 1A8 (anti-Ly6G) or isotype control (2A3) Ab from 5 weeks of age, and sacrificed 50 days later. (**D**) Number of polyps per mouse. (**E**) Representative sections of adenomas immunostained with Ab against MPO (brown), counterstained with hematoxylin, and visualized by light microscopy. Arrows denote clusters of MPO⁺ cells. Original magnification, ×200. (**F**) Number of MPO⁺ neutrophils per polyp section. (**G**) Microvessel density in adenomas ($n$ = 5–6 per group). *$P$ < 0.05, **$P$ < 0.01, ***$P$ < 0.001, Mann-Whitney test. Box and whisker plots show median (lines within boxes), interquartile range (bounds of boxes), and upper and lower range (whiskers).

AOM/DSS tumorigenesis to a similar extent, but it was notable that, unlike *Cxcr2* deficiency, Ly6G⁺ cell depletion had no effect on tumor microvessel density (Figure 11C).

Similar experiments were then performed in $Apc^{Min/+}$ mice (Figure 11, D–G): 35-day-old animals received 1A8 or isotype control 3 times per week, and their intestines were analyzed 7 weeks later. Like CXCR1/2 pepducin treatment, this prolonged Ly6G⁺ cell depletion led to a significant reduction in the number of intestinal adenomas in $Apc^{Min/+}$ mice compared with animals receiving isotype control (Figure 11D). MPO⁺ cells were absent from the tumors that developed in 1A8-treated $Apc^{Min/+}$ mice (Figure 11, E and F), but tumor microvessel density was no different from that of controls (Figure 11G). 1A8 and CXCR1/2 pepducin reduced polyp burden to a similar extent in $Apc^{Min/+}$ mice; combining the treatments failed to suppress adenoma development beyond that seen with either treatment alone (data not shown). Thus, long-term Ly6G⁺ cell depletion reduced the number of adenoma-associated MPO⁺ cells, but had no effect on tumor microvessel density. However, it suppressed formation of AOM/DSS-induced and spontaneous $Apc^{Min/+}$ adenomas to a similar extent as CXCR2 deficiency or inhibition.

*Short-term Ly6G⁺ cell depletion suppresses papilloma growth and enhances tumor cell apoptosis.* Next, we sought to determine whether short-term 1A8 treatment could be used to deplete tumor-associated MPO⁺ cells and allow us to explore their role in controlling the growth of established tumors. We used mice carrying DMBA/TPA-induced papillomas so that we could noninvasively measure the size of individual tumors before and after Ly6G⁺ cell depletion. These mice were treated with 1A8 or 2A3 3 times per week for 2.5 weeks. Blood Gr1⁺ cells were reduced in 1A8-treated mice at the time of harvest, as expected, and the papillomas taken from these animals contained far fewer cells expressing MPO (by immunohistochemistry) or Gr1 (by flow cytometry) than tumors from 2A3-treated mice (Figure 12A and data not shown). Moreover, by comparing the size of individual tumors and the total tumor burden before and after Ab treatment, it was apparent that Ly6G⁺ cell depletion was accompanied by a marked suppression of papilloma growth (Figure 12B). Ly6G⁺ cell depletion had no effect on intratumoral microvessel density (Figure 12C), on tumor cell expression of p53 or p16, or on incorporation of BrdU into the cells of the papilloma (Supplemental Figure 11). However, papillomas from 1A8-treated mice contained far more cells positive for cleaved caspase 3 than did tumors from isotype-treated animals (Figure 12, D and E), indicative of increased tumor cell death. Thus, short-term anti-Ly6G Ab treatment depleted tumor-associated MPO⁺ cells; had no effect on tumor microvessel density; enhanced tumor cell death; and suppressed papilloma growth.

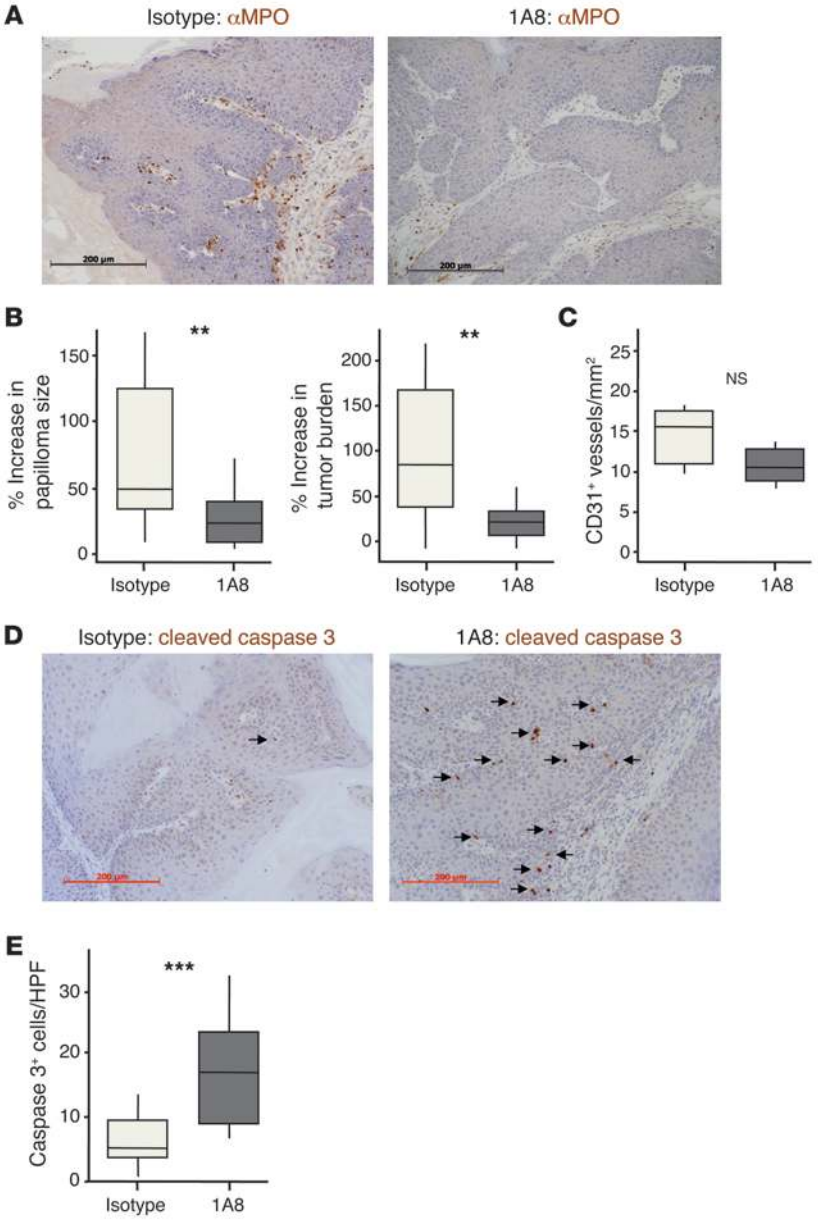


**Figure 12**
Ly6G$^+$ cell depletion suppresses growth of established papillomas. Papilloma-bearing WT mice were treated 3 times per week for 2.5 weeks with 1A8 (anti-Ly6G) or isotype control (2A3) Ab. Papillomas were measured before and after Ab treatment. (**A**) Representative sections of papillomas immunostained with anti-MPO (brown), counterstained with hematoxylin, and visualized by light microscopy. (**B**) Increase in papilloma size and tumor burden over the course of Ab treatment. (**C**) Microvessel density ($n$ = 5–6 per group). (**D**) Representative sections of papillomas immunostained with anti–cleaved caspase 3 Ab (brown), counterstained with hematoxylin, and visualized by light microscopy. Arrows denote cleaved caspase 3–positive cells. (**E**) Average number of cleaved caspase 3–positive cells per high-powered field. $^{**}P < 0.01$, $^{***}P < 0.01$, Mann-Whitney test. Scale bars: 200 μm. Box and whisker plots show median (lines within boxes), interquartile range (bounds of boxes), and upper and lower range (whiskers).

## Discussion

Chemokine expression is often dysregulated during carcinogenesis, and oncogene activation leads to induction of proinflammatory chemokines (16, 42, 43). However, the promiscuity of chemokines and their receptors has led to the view that while inhibition of a single chemokine receptor might have some effect on primary tumor formation, the functional redundancy built into the chemokine system to ensure robust responses during infection will limit the effect that any single chemokine receptor will have on de novo tumor development. Indeed, there are only a few reports of genetic chemokine receptor deficiency altering susceptibility to primary tumor formation in spontaneous mouse models of cancer (28, 44), and some components of chemokine networks known to influence inflammation-driven tumorigenesis (e.g., CCL2 and D6) are likely to be regulating responses to exogenous inflammatory agents rather than modifying the stroma of established tumors (27, 45–47). For example, D6 deficiency, despite enhancing AOM/DSS-induced tumorigenesis (46), has no effect on spontaneous adenoma formation in *Apc*$^{Min/+}$ mice, and induction of D6 transgenes does not affect the growth of established papillomas (O.J. Sansom and R.J.B. Nibbs, unpublished observations), despite similar transgenes suppressing papillomagenesis when they are present throughout tumor induction (45). The effect of CXCR2 deficiency on tumor susceptibility is therefore particularly notable because of (a) the extent of tumor suppression, (b) its effect on both inflammation-driven and spontaneous tumor formation, and (c) its role in tumorigenesis in multiple tissues (i.e., skin, small intestine, colon, and oral cavity).

We contend that this is primarily because the recruitment of blood Ly6G$^+$ cells, which can give rise to tumor-associated MPO$^+$ cells, was heavily dependent on CXCR2 (i.e., there is minimal functional redundancy), and that these cells were key players in tumori-

genesis in all the models we examined. This is based on several observations. First, there was no alternative signaling receptor for most of the CXCR2 ligands in mice. Second, CXCR2 was highly restricted to Ly6G$^+$ cells in blood, and leukocytes were the dominant source of CXCR2 in inflamed tissues and tumors. Third, CXCR2 was indispensable for the accumulation of MPO$^+$ cells in inflamed tissues and tumors. Fourth, Ly6G$^+$ cell depletion suppressed adenoma development in *Apc*$^{Min/+}$ and AOM/DSS-treated mice to an extent similar to that of CXCR2 inhibition/deficiency, without noticeably affecting tumor microvessel density. Fifth, combining pepducin-mediated CXCR2 inhibition and Ly6G$^+$ cell depletion had no additive effect in *Apc*$^{Min/+}$ mice. Sixth, Ly6G$^+$ cell depletion slowed the growth of established papillomas, without altering tumor microvessel density.

Although no CXCR2 immunoreactivity on epithelial or endothelial cells in inflamed tissues or tumors was detected, it is possible that CXCR2 on these cells affects tumorigenesis. CXCR2 on endothelial cells can mediate angiogenesis (14), and there were clear reductions in microvessel density in tumors in *Cxcr2*$^{-/-}$ mice in the DMBA/TPA and AOM/DSS models. Notably, this was not seen after Ly6G$^+$ cell depletion from *Apc*$^{Min/+}$ mice, WT mice with DMBA/TPA-induced papillomas, or AOM/DSS-treated WT mice; therefore, the reduced microvessel density of *Cxcr2*$^{-/-}$ tumors is probably independent of defects in Ly6G$^+$ cell recruitment, and more likely caused by loss of direct CXCR2-mediated regulation of endothelial cells. Interestingly, although CXCR1/2 pepducin prevented accumulation of MPO$^+$ cells in *Apc*$^{Min/+}$ adenomas, it had no effect on microvessel density, which suggests that the activity of CXCR1/2 pepducin is limited to leukocytic CXCR2, perhaps because it is unable to access CXCR2 on tumor-associated endothelial cells.

We attempted to specifically address the protumorigenic role of hemopoietic CXCR2 using bone marrow radiation chimeras (data not shown). Radiation chimerism is a complex experimental system requiring key control groups, and we encountered several problems that precluded definitive conclusions, including the death of all KO→KO and greater than 50% of all WT→KO and KO→WT chimeras, by 6 weeks after irradiation (similar problems have been reported by others; ref. 48) and the reacquisition of substantial numbers of CXCR2-expressing (i.e., WT) Gr1$^{hi}$ blood cells 10–20 weeks after irradiation (the period of tumor induction) in surviving KO→WT chimeras. The extent of recipient chimerism is not reported in other studies using CXCR2 KO→WT chimeras (15, 48–50), but will clearly influence data interpretation. In addition, not all WT→WT and WT→KO chimeras developed tumors, and those that did had far fewer than unirradiated WT animals. Thus, irradiation per se altered tumor susceptibility, so that KO→KO mice, and KO→WT mice without WT blood cells, were critical for interpreting WT→WT and WT→KO data. Definitive roles for CXCR2 on different cell types remain to be determined, and we are developing *Cxcr2*$^{fl/fl}$ mice to give temporal and lineage-specific control over *Cxcr2* deletion and allow us to answer this question.

The role of CXCR2 in senescence in vivo also requires investigation (21). It seems unlikely to be playing a major role in the models we studied here, but it could allow CXCR2 to act as a tumor suppressor in some contexts, particularly in models more clearly associated with senescence, such as after PTEN inactivation in prostate, or BRAF activation in melanocytes (51, 52). However, it should be noted that the CXCR2/senescence study was performed in vitro in the absence of immune cells, and secretion of CXCR2 ligands was an important component of the response (21). In vivo, this would be expected to initiate local inflammation, which could mask any senescence-related tumor suppressor effects mediated by CXCR2. Again, *Cxcr2*$^{fl/fl}$ mice will be valuable tools in helping to study this putative function of CXCR2 in vivo.

In inflammation-driven cancer models, CXCR2 deficiency substantially altered responses to TPA and DSS, and this likely contributed to tumor suppression. Nonetheless, all DMBA/TPA-induced papillomas and AOM/DSS-induced adenomas evolved high, constitutive expression of CXCL1, CXCL2, CXCL5, and/or CXCL7 that was maintained long after treatment with inflammatory agents had been discontinued. In papillomas, these chemokines were made by stromal and tumor cells, and both DMBA/TPA-induced papillomas and AOM/DSS-induced adenomas showed CXCR2-dependent accumulation of MPO$^+$ cells. These cells were of functional importance, because short-term Ly6G$^+$ cell depletion, which purged tumor-associated MPO$^+$ cells, slowed the growth of established skin papillomas. These observations point toward an indispensable role for CXCR2-mediated leukocyte recruitment in *tumor-driven* inflammation, and this is given further credence by the data from spontaneous tumor models. The near-complete suppression of tumorigenesis by *Cxcr2* deletion in *AhCreER;Apc*$^{fl/+}$*;Pten*$^{fl/fl}$ mice was unexpected. There were no immediate CXCR2-dependent consequences of *Pten* and/or *Apc* deletion, but all tumors examined contained substantial populations of MPO$^+$ cells and had upregulated at least 1, and often all 4, of the CXCR2 ligands. Analysis of *Apc*$^{Min/+}$ adenoma cultures showed that CXCL1, CXCL2, CXCL5, and CXCL7 were major components of the adenoma secretome and that there was not widespread induction of non–CXCR2-binding chemokines. It therefore appears that specific production of CXCR2 ligands is a universal property of skin and intestinal tumors in the models we used, which suggests that there is strong selective pressure for the emergence of this characteristic during tumor development.

Leukocytes are the main source of CXCR2 in inflamed tissues and tumors, and CXCR2 is highly restricted to Ly6G$^+$ cells in blood. Before tumor development, these Ly6G$^+$ cells are mainly neutrophils. Some recent studies on tumor-associated neutrophils support a protumorigenic role for these cells in primary tumors (53–57), and our present data suggested that acute CXCR2-driven neutrophil recruitment influences epithelial cell proliferation in the skin and gut in response to inflammatory stimuli. This could also play a role in the spontaneous models, where one might envisage very early tumors recruiting neutrophils through CXCR2 to support their proliferative expansion. In established papillomas, however, it was tumor cell death that was most noticeably affected by Ly6G$^+$ cell depletion, so perhaps the manner in which these cells support tumorigenesis changes as the tumor develops. Alternatively, the type of cells recruited by CXCR2 ligands may change. In tumor-bearing mice, circulating neutrophil numbers increase, but there are also changes in myeloid development, such that circulating Gr1$^+$CD11b$^+$ MDSC populations emerge that resemble neutrophil precursors found in the bone marrow of tumor-free mice (32). Many of these cells, particularly polymorphonuclear MDSCs, will have the potential to be recruited to tumors by CXCR2 engagement (11). Interestingly, we only saw increased numbers of cleaved caspase 3$^+$ tumor cells after Ly6G$^+$ cell depletion from mice with established tumors. The few inflammation-driven or spontaneous tumors that emerged after long-term Ly6G$^+$ cell depletion, CXCR2 deficiency, or CXCR2 inhibition did not contain more cleaved

caspase 3$^+$ tumor cells than did controls (Supplemental Figure 2B and Supplemental Figure 12), presumably because they developed survival strategies that did not rely on CXCR2$^+$ cells.

Neutrophils and polymorphonuclear MDSCs carry a wealth of molecules that might contribute to their protumorigenic activity, such as DNA-damaging reactive oxygen species and protumorigenic cytokines (e.g., TNF-α and IL-6) (58, 59). They also release proteases (e.g., elastase and matrix metalloproteinases) that can directly regulate tumor cell proliferation and modify the tumor stroma (56, 57, 60). These proteases might aid tumor invasion, and it was notable that MPO$^+$ cells were often found at the invasive front of *AhCreER;Apc$^{fl/+}$;Pten$^{fl/fl}$* tumors and that far fewer tumors in *AhCreER;Apc$^{fl/+}$;Pten$^{fl/fl}$;Cxcr2$^{-/-}$* mice were invasive. This might be due to slowed tumor development, but evidence already exists that chemokines can control local invasion by recruiting leukocytes to the invasive front (11, 61, 62). For example, CCL9, acting through CCR1, aids intestinal tumor invasion and liver metastasis in *cis-Apc$^{+/\Delta 716}$;Smad4$^{+/-}$* mice by this mechanism (63, 64). Chemokine receptors on leukocytes have also been implicated in facilitating the formation of secondary tumor deposits (65). In this regard, it is interesting that, in contrast to the protumorigenic roles of neutrophils in primary tumors, "tumor-educated" neutrophils have been reported to suppress the formation of metastatic deposits in the lung (66). A role for CXCR2 in directing the homing of these cells is possible, and needs to be explored.

Collectively, our data suggest that CXCR2 might be an efficacious target in the prevention of inflammation-associated cancers and the treatment of established tumors. A variety of small molecule CXCR2 antagonists have already been developed, ostensibly for the treatment of inflammatory disease (25), so it should be possible to rapidly explore their activity in preclinical models of cancer. In this respect, it is encouraging that pepducins inhibited adenoma formation in *Apc$^{Min/+}$* mice (present study), pancreatic ductal adenocarcinoma progression can be suppressed with a CXCR2 inhibitor (26), and humanized neutralizing Ab against CXCL8 (a human-specific CXCR2 ligand) reduce tumor burden in animal models of melanoma (67). However, on a cautionary note, CXCR2$^+$ neutrophils play a critical role in immune defense, so inhibiting their homing is likely to lead to increased susceptibility to infection. Neutropenia is also a significant concern during chemotherapy. Moreover, if neutrophils can suppress the formation of metastatic deposits (66), then CXCR2 antagonism could enhance cancer spread. Nonetheless, within the chemokine receptor family, we propose that CXCR2 is currently the most encouraging candidate as a target for cancer therapy or prophylaxis.

## Methods

*Mice*. Mice were maintained in specific pathogen–free conditions at the Beatson Institute for Cancer Research or Glasgow University animal facilities. All experiments were performed on a BALB/c background, apart from *Apc$^{Min/+}$* mice (C57BL/6J), and *AhCreER;Apc$^{fl/fl}$;Pten$^{fl/fl}$* and *K14CreER;KRas$^{G12D/+}$* animals (mixed background: 50% BALB/c, 25% C57BL/6J, and 25% S129), and inbred FVB mice (Charles River) were used in the papilloma neutrophil depletion studies. *Cxcr2$^{-/-}$* mice weighing greater than 20% less than age-matched WT animals were excluded from the study.

*Neutrophil depletion and blood neutrophil quantitation*. For neutrophil depletion studies, 500 μg of either 1A8 monoclonal Ab (anti-mLy-6G; Bioxcell) or 2A3 isotype control Ab (Rat IgG2a; Bioxcell) was injected i.p. either once or 3 times per week for the duration of the experiment, as indicated. To evaluate neutrophil/Ly6G$^+$ cell depletion, 200–500 μl blood was collected by cardiac puncture into EDTA-containing tubes, and neutrophils were enumerated (per milliliter blood and as a percentage of wbcs) using an ADVIA 2120 Hematology System (Siemens), according to the manufacturer's instructions. Blood samples were also analyzed by flow cytometry after staining with fluorescent Ab against CXCR2, CD11b, and Gr1 or Ly6G (see below).

*Skin inflammation and papillomas*. Skin inflammation was induced by applying TPA (Sigma-Aldrich) to shaved dorsal skin as previously described (45). Skin was harvested at various times after a single TPA application (acute inflammation), or after the last of 6 TPA applications (3 per week) (chronic inflammation). Skin papillomas were induced as described previously (45), with a single application of 25 μg of DMBA (Sigma-Aldrich) followed by triweekly TPA treatments for up to 22 weeks. The incidence and number of papillomas per mouse was scored weekly; papillomas in excess of 1 mm$^2$ and clearly raised above the adjacent unaffected skin were counted. At the end of the experiment, the area occupied by individual papillomas was calculated (in mm$^2$) using calliper measurements, and tumors were processed for histological or RNA analysis. For neutrophil depletion experiments, FVB mice were treated with DMBA, followed by triweekly TPA applications for 12 weeks, to induce a moderate papilloma burden. 1A8 or 2A3 control Ab was then injected i.p. 3 times per week for a further 2.5 weeks. The size of individual tumors was determined before and after Ab treatment, and the percent change in the size of individual tumors or overall tumor burden was calculated.

*Colitis and colitis-associated tumors*. For colitis experiments, mice were provided ad libitum with 2% or 3.5% (w/v) DSS (MP Biomedicals, MW 36–50 kDa) in place of their drinking water for 5 days, after which normal drinking water was given. Clinical symptoms of disease were scored as previously described (68). To induce colitis-associated cancer (Supplemental Figure 3), mice were injected i.p. with 12.5 mg/kg AOM (Sigma-Aldrich), followed 3 days later by 3 cycles of 2% DSS (for 5 days) and normal drinking water (for 16 days). Animals were sacrificed 70 days after AOM injection, and colons were harvested. For neutrophil depletion experiments, mice received 500 μg of either 1A8 or 2A3 control Ab i.p. 3 times per week from the start of the first DSS feed, and sacrificed at the end of the second cycle of DSS feeding.

*Pepducin treatment and neutrophil depletion in Apc$^{Min/+}$ mice*. For pepducin treatments, 35-day-old *Apc$^{Min/+}$* mice were injected s.c. with 2.5 mg/kg ×1/2pal-i3 pepducin (RTLFKAHMGQKHR, palmitoyl N-terminal, amidation C-terminal; Genscript; ref. 24) or control ×1/2pal-i3CONT pepducin (TRFLAKMHQGHKR, palmitoyl N-terminal, amidation C-terminal; Genscript; ref. 24) in sterile saline, and then daily with 1 mg/kg ×1/2pal-i3 or ×1/2pal-i3CONT. For neutrophil depletion, 35-day-old *Apc$^{Min/+}$* mice were injected i.p. 3 times per week with 500 μg 1A8 or 2A3 isotype control. Animals were sacrificed when they were 85 days old, and small intestines were harvested.

*AhCreER;Apc$^{fl/fl}$;Pten$^{fl/fl}$ mice*. For short-term experiments, *AhCreER;Apc$^{fl/fl}$;Pten$^{fl/fl}$;Cxcr2$^{+/+}$* and *AhCreER;Apc$^{fl/fl}$;Pten$^{fl/fl}$;Cxcr2$^{-/-}$* mice were injected i.p. with 80 mg/kg tamoxifen and 80 mg/kg β-naphthoflavone in corn oil on 4 consecutive days and sacrificed 4 or 6 days after the final injection. Tumors were induced in *AhCreER;Apc$^{fl/+}$;Pten$^{fl/fl}$;Cxcr2$^{+/+}$* and *AhCreER;Apc$^{fl/+}$;Pten$^{fl/fl}$;Cxcr2$^{-/-}$* mice by i.p. injection of 80 mg/kg tamoxifen and 80 mg/kg β-naphthoflavone in corn oil either once or on 4 consecutive days. Mice were sacrificed 50–200 days after cre induction or when they showed moderate signs of illness. Colons and small intestines were harvested at the end of all experiments.

*Oral papillomas*. The oral mucosa of *K14CreER;KRas$^{G12D/+}$;Cxcr2$^{+/+}$* and *K14CreER;KRas$^{G12D/+}$;Cxcr2$^{+/-}$* mice (39) was closely inspected on a daily basis. Owing to their intrabuccal location, it was not possible to directly measure papilloma size. Since oral papillomas interfered with feeding, body weight of affected mice was monitored. Mice were sacrificed when their body weight dropped to 80% of that of papilloma-free littermates. Heads of sacrificed mice were halved sagittally and processed whole for histol-

ogy, or tumors were dissected out and snap-frozen for RNA and protein extraction. Life span data was used to generate Kaplan-Meier survival plots.

*Human adenomas*. Sections of formalin-fixed paraffin-embedded human adenomas were prepared and archived, with appropriate ethical approval, at the Department of Pathology, Ludwig-Maximilians-Universität, Munich, Germany.

*Tissue processing, immunohistochemistry, and LCM*. Tissue samples were fixed in either methacarn (methanol/chloroform/acetic acid; 4:2:1) or 10% neutral buffered formalin, embedded in paraffin wax, and sectioned. Sections were either stained with H&E or immunostained using standard immunohistochemical protocols. The following Abs were used: anti-mouse CXCR2 (clone 242216; R&D Systems); anti-MPO (A0398; Dako); anti-BrdU (N347580; Becton Dickinson), which was used when mice had been injected i.p. with 250 μl Cell Proliferation Labelling Reagent (GE Healthcare) 2 hours before harvest; anti-p53 (CM5; Vector labs); anti-p16 (SC1661; Santa Cruz); anti-p21 (MI9; Santa Cruz); anti–active caspase 3 (R&D Systems); anti-γH2ax (05636; Millipore); anti-Ki67 (VP-K452; Vector labs); anti–β-catenin (C19220; Transduction Laboratories); anti–p-Akt Ser473 (4060XP; Cell Signaling) and anti-CD31 (28364; Abcam). To determine microvessel density, anti-CD31–stained tumor sections were examined at ×40 magnification by an investigator blinded to their identity, and intratumoral $CD31^+$ vessels were counted. At least 3 tumors were examined per mouse to give a score of microvessel density per square millimeter of tumor, and at least 5 mice were scored per group. For LCM, papillomas were snap frozen in liquid nitrogen and stored in OCT embedding medium (CellPath) at –80°C. 35-μm sections were mounted on Leica LCM slides. At ×40 power on a Leica LMD 6500 microscope, papilloma epithelium and stroma were individually isolated and immediately stored in extraction buffer from the Arcturus Picopure RNA isolation kit (Applied Biosystems), and this kit was used to extract RNA.

*Flow cytometry*. Blood was collected as described above, and rbcs were lysed in 0.8% $NH_4Cl$, 0.1 mM EDTA for 10 minutes on ice. Bone marrow was isolated from femurs using 3 ml RPMI (plus 10% FCS) delivered with a 5-ml syringe fitted with a 21-gauge needle, and the cells were washed once in RPMI containing 10% FCS. Papillomas were minced in PBS and incubated for 100 minutes at 37°C in 5 ml HBSS containing 1 mg/ml collagenase D and 30 μg/ml DNAse I. 3 mg/ml Dispase (Invitrogen) was added, and samples were incubated for a further 15 minutes at 37°C before being passed through a 70-μm cell strainer, collected by centrifugation, and resuspended in RPMI (supplemented with 10% FCS). In preparation for flow cytometry, all samples were washed once with FACS buffer (PBS plus 2% FCS and 5 mM EDTA) and blocked with rat anti-mouse CD16/CD32 in FACS buffer for 20 minutes at 4°C. After washing once with FACS buffer, cells were immunostained as appropriate with the following rat anti-mouse monoclonal Abs: phycoerythrin-coupled anti-CXCR2 (242216; R&D Systems), fluorescein isothiocyanate-coupled anti-Gr1 (RB6-8C5; eBioscience), fluorescein isothiocyanate- or allophycocyanin/cyanine-7–coupled anti-CD11b (M1/70; BD Biosciences), allophycocyanin/cyanine-7–coupled anti-Ly6G (1A8; BD Biosciences), and/or appropriately labeled isotype controls (BD Biosciences). Dead cells were labeled with Viaprobe (BD Biosciences) and excluded during analysis. Ab-labeled cells were analyzed using a MACSQuant cytometer (Miltenyi). Data were analyzed using FlowJo (Treestar) with populations defined using size, viability, and "fluorescence minus one" isotype controls.

*Q-RT-PCR*. Tissue samples for RNA analysis were collected in RNAlater (Sigma-Aldrich), and mRNA was isolated by homogenization in TRIzol (Invitrogen) using an Ultraturrax T18 basic tissue homogenizer (IKA) set at 23,000 rpm. RNA was further purified using DNA-free (Ambion). 500 ng RNA was reverse transcribed using Affinity Script Reverse Transcriptase kit (Stratagene), according to the manufacturer's instructions. Transcripts were measured by Q-RT-PCR on a 7900HT Fast-Real Time PCR System (Applied Biosystems), fitted with sequence detection software SDS 2.3, using TaqMan gene expression assays (Applied Biosystems) for CXCL1 (Mm00433859_m1), CXCL2 (Mm00436450_m1), CXCL5 (Mm00436451_g1), CXCL7 (Mm00470163_m1), and CXCR2 (Mm00438258_m1), including GAPDH (4352932E) as an endogenous control. Thermal cycle conditions were 95°C for 10 minutes, followed by 40 cycles of 95°C for 15 seconds, and 60°C for 1 minute. To control for contamination, Q-RT-PCR reactions were performed using water in place of cDNA and using samples in which reverse transcriptase had been omitted from the cDNA synthesis step. Data sets were analyzed only when these samples generated no signal during the Q-RT-PCR reaction. Relative expression between samples was determined using the $\Delta\Delta C_t$ method using RQ Manager. Data are presented as relative expression of each gene, with the mean of control samples set to 1.

*Intestinal crypt and adenoma culture*. Intestinal crypts were isolated from WT C57BL/6 mice using the proximal 10 cm of the small intestine and cultured in Growth Factor Reduced Matrigel (BD Biosciences) in Advanced DMEM/F12 medium (containing 10 mM HEPES, pH 7.4; 5 mM glutamine; N-2 Supplement, 1:100 dilution; and B-27 Supplement, 1:50 dilution; all from Invitrogen), with 50 ng/ml epidermal growth factor (Peprotech), 100 ng/ml Noggin (Peprotech), and 500 ng/ml R-spondin 1 (R&D Systems), essentially as previously described (69). Adenomas from the small intestine of $Apc^{Min/+}$ mice were isolated, pooled, washed, and digested in 2.5% trypsin/100 U DNase for 30 minutes at 37°C. Cells were allowed to form spheroids in Matrigel and medium (described above), with 50 ng/ml epidermal growth factor and 100 ng/ml Noggin included in the medium. For both crypt and adenoma cultures, fresh growth factors were added every other day, and the whole culture medium was changed every 3–4 days. Conditioned medium and cells were harvested and analyzed after 7 days of culture.

*ELISA and protein arrays*. Tissues and tumors were weighed, then homogenized in a small volume of Tissue Protein Extraction Reagent (Thermo Scientific) supplemented with protease inhibitor cocktail (Thermo Scientific) for 15 minutes at 22°C in a Tissue-Lyser (Qiagen), according to the manufacturers' protocols. CXCL1, CXCL2, and CXCL5 concentrations were measured using DuoSet ELISAs (R&D Systems) and are presented as amount of chemokine per milligram tissue/tumor. Chemokines in conditioned media from crypt and adenoma cultures were also quantified using this method. 100 μl of these conditioned media were also analyzed on RayBio Mouse Cytokine Antibody Arrays (RayBiotech), according to the manufacturer's instructions. Fluorescent signals were detected, quantified, and analyzed on a ScanArray Express Microarray Scanner (Packard Bioscience).

*Statistics*. Data were analyzed using GraphPad Prism 4 or Minitab software using 1-way ANOVA (with multiple comparison post-test), Mann-Whitney test, or log-rank test, as indicated in the figure legends. A $P$ value less than 0.05 was considered significant.

*Study approval*. All experiments received ethical approval and were performed under the auspices of UK Home Office licences.

## Acknowledgments

The Medical Research Council and Cancer Research UK supported this work. C.W. Steele is a Wellcome Trust Clinical Research Fellow. Work in R.J.B. Nibbs's lab is funded in part by a Medical Research Council Programme grant. R.J.B. Nibbs acknowledges support services provided by A. Wilson.

Received for publication September 29, 2011, and accepted in revised form July 2, 2012.

Address correspondence to: Robert J.B. Nibbs, Institute of Infection, Immunity, and Inflammation, College of Medical, Veteri-

nary, and Life Sciences, Glasgow Biomedical Research Centre, 120 University Place, University of Glasgow, Glasgow G12 8TA, United Kingdom. Phone: 44.141.330.3960; Fax: 44.141.330.4297; E-mail: Robert.Nibbs@glasgow.ac.uk. Or to: Owen J. Sansom, Beatson Institute of Cancer Research, Garscube Estate, Switchback Road, Glasgow G61 1BD, United Kingdom. Phone: 44.141.330.3953; Fax: 44.141.942.6521; E-mail: o.sansom@beatson.gla.ac.uk.

Michael S. Samuel's present address is: Centre for Cancer Biology, SA Pathology, Adelaide, Australia.

1. Mantovani A, Allavena P, Sica A, Balkwill F. Cancer-related inflammation. *Nature*. 2008; 454(7203):436–444.
2. Coussens LM, Werb Z. Inflammation and cancer. *Nature*. 2002;420(6917):860–867.
3. Xie J, Itzkowitz SH. Cancer in inflammatory bowel disease. *World J Gastroenterol*. 2008;14(3):378–389.
4. Iwama T. NSAIDs and colorectal cancer prevention. *J Gastroenterol*. 2009;44(Suppl 19):72–76.
5. Galon J, et al. Type, density, and location of immune cells within human colorectal tumors predict clinical outcome. *Science*. 2006;313(5795):1960–1964.
6. Balkwill F. Cancer and the chemokine network. *Nat Rev Cancer*. 2004;4(7):540–550.
7. Rot A, von Andrian UH. Chemokines in innate and adaptive host defense: basic chemokinese grammar for immune cells. *Annu Rev Immunol*. 2004; 22:891–928.
8. Fan X, et al. Murine CXCR1 is a functional receptor for GCP-2/CXCL6 and interleukin-8/CXCL8. *J Biol Chem*. 2007;282(16):11658–11666.
9. Cacalano G, et al. Neutrophil and B cell expansion in mice that lack the murine IL-8 receptor homolog. *Science*. 1994;265(5172):682–684.
10. Fridlender ZG, et al. Polarization of tumor-associated neutrophil phenotype by TGF-beta: "N1" versus "N2" TAN. *Cancer Cell*. 2009;16(3):183–194.
11. Yang L, et al. Abrogation of TGF beta signaling in mammary carcinomas recruits Gr-1+CD11b+ myeloid cells that promote metastasis. *Cancer Cell*. 2008;13(1):23–35.
12. Sawanobori Y, et al. Chemokine-mediated rapid turnover of myeloid-derived suppressor cells in tumor-bearing mice. *Blood*. 2008;111(12):5457–5466.
13. Heidemann J, et al. Angiogenic effects of interleukin 8 (CXCL8) in human intestinal microvascular endothelial cells are mediated by CXCR2. *J Biol Chem*. 2003;278(10):8508–8515.
14. Strieter RM, Burdick MD, Mestas J, Gomperts B, Keane MP, Belperio JA. Cancer CXC chemokine networks and tumour angiogenesis. *Eur J Cancer*. 2006;42(6):768–778.
15. Reutershan J, et al. Critical role of endothelial CXCR2 in LPS-induced neutrophil migration into the lung. *J Clin Invest*. 2006;116(3):695–702.
16. Sparmann A, Bar-Sagi D. Ras-induced interleukin-8 expression plays a critical role in tumor growth and angiogenesis. *Cancer Cell*. 2004;6(5):447–458.
17. Cataisson C, et al. Inducible cutaneous inflammation reveals a protumorigenic role for keratinocyte CXCR2 in skin carcinogenesis. *Cancer Res*. 2009;69(1):319–328.
18. Luan J, et al. Mechanism and biological significance of constitutive expression of MGSA/GRO chemokines in malignant melanoma tumor progression. *J Leukoc Biol*. 1997;62(5):588–597.
19. Maxwell PJ, et al. HIF-1 and NF-kappaB-mediated upregulation of CXCR1 and CXCR2 expression promotes cell survival in hypoxic prostate cancer cells. *Oncogene*. 2007;26(52):7333–7345.
20. Wang B, Hendricks DT, Wamunyokoli F, Parker MI. A growth-related oncogene/CXC chemokine receptor 2 autocrine loop contributes to cellular proliferation in esophageal cancer. *Cancer Res*. 2006; 66(6):3071–3077.
21. Acosta JC, et al. Chemokine signaling via the CXCR2 receptor reinforces senescence. *Cell*. 2008; 133(6):1006–1018.
22. Murphy C, et al. Nonapical and cytoplasmic expression of interleukin-8, CXCR1, and CXCR2 correlates with cell proliferation and microvessel density in prostate cancer. *Clin Cancer Res*. 2005; 11(11):4117–4127.
23. Acosta JC, Gil J. A role for CXCR2 in senescence, but what about in cancer? *Cancer Res*. 2009; 69(6):2167–2170.
24. Kaneider NC, Agarwal A, Leger AJ, Kuliopulos A. Reversing systemic inflammatory response syndrome with chemokine receptor pepducins. *Nat Med*. 2005;11(6):661–665.
25. Dwyer MP, Biju P. Discovery of 3,4-diaminocyclobut-3-ene-1,2-dione-based CXCR2 receptor antagonists for the treatment of inflammatory disorders. *Curr Top Med Chem*. 2010;10(13):1339–1350.
26. Ijichi H, et al. Inhibiting Cxcr2 disrupts tumor-stromal interactions and improves survival in a mouse model of pancreatic ductal adenocarcinoma. *J Clin Invest*. 2011;121(10):4106–4117.
27. O'Hayer KM, Brady DC, Counter CM. ELR+ CXC chemokines and oncogenic Ras-mediated tumorigenesis. *Carcinogenesis*. 2009;30(11):1841–1847.
28. Shen H, Schuster R, Lu B, Waltz SE, Lentsch AB. Critical and opposing roles of the chemokine receptors CXCR2 and CXCR3 in prostate tumor growth. *Prostate*. 2006;66(16):1721–1728.
29. Young AR, et al. Autophagy mediates the mitotic senescence transition. *Genes Dev*. 2009;23(7):798–803.
30. Lagasse E, Weissman IL. Flow cytometric identification of murine neutrophils and monocytes. *J Immunol Methods*. 1996;197(1–2):139–150.
31. Daley JM, Thomay AA, Connolly MD, Reichner JS, Albina JE. Use of Ly6G-specific monoclonal antibody to deplete neutrophils in mice. *J Leukoc Biol*. 2008;83(1):64–70.
32. Gabrilovich DI, Ostrand-Rosenberg S, Bronte V. Coordinated regulation of myeloid cells by tumours. *Nat Rev Immunol*. 2012;12(4):253–268.
33. Fan GH, Lapierre LA, Goldenring JR, Richmond A. Differential regulation of CXCR2 trafficking by Rab GTPases. *Blood*. 2003;101(6):2115–2124.
34. Baugher PJ, Richmond A. The carboxyl-terminal PDZ ligand motif of chemokine receptor CXCR2 modulates post-endocytic sorting and cellular chemotaxis. *J Biol Chem*. 2008;283(45):30868–30878.
35. Buanne P, et al. Crucial pathophysiological role of CXCR2 in experimental ulcerative colitis in mice. *J Leukoc Biol*. 2007;82(5):1239–1246.
36. Farooq SM, Stillie R, Svensson M, Svanborg C, Strieter RM, Stadnyk AW. Therapeutic effect of blocking CXCR2 on neutrophil recruitment and dextran sodium sulfate-induced colitis. *J Pharmacol Exp Ther*. 2009;329(1):123–129.
37. Su LK, et al. Multiple intestinal neoplasia caused by a mutation in the murine homolog of the APC gene. *Science*. 1992;256(5057):668–670.
38. Marsh V, et al. Epithelial Pten is dispensable for intestinal homeostasis but suppresses adenoma development and progression after Apc mutation. *Nat Genet*. 2008;40(12):1436–1444.
39. Raimondi AR, Molinolo A, Gutkind JS. Rapamycin prevents early onset of tumorigenesis in an oral-specific K-ras and p53 two-hit carcinogenesis model. *Cancer Res*. 2009;69(10):4159–4166.
40. Samuel MS, Lourenco FC, Olson MF. K-Ras mediated murine epidermal tumorigenesis is dependent upon and associated with elevated Rac1 activity. *PLoS One*. 2011;6(2):e17143.
41. Dietrich WF, et al. Genetic identification of Mom-1, a major modifier locus affecting Min-induced intestinal neoplasia in the mouse. *Cell*. 1993;75(4):631–639.
42. Soucek L, Lawlor ER, Soto D, Shchors K, Swigart LB, Evan GI. Mast cells are required for angiogenesis and macroscopic expansion of Myc-induced pancreatic islet tumors. *Nat Med*. 2007;13(10):1211–1218.
43. Ji H, et al. K-ras activation generates an inflammatory response in lung tumors. *Oncogene*. 2006; 25(14):2105–2112.
44. Shen H, Schuster R, Stringer KF, Waltz SE, Lentsch AB. The Duffy antigen/receptor for chemokines (DARC) regulates prostate tumor growth. *FASEB J*. 2006;20(1):59–64.
45. Nibbs RJ, et al. The atypical chemokine receptor D6 suppresses the development of chemically induced skin tumors. *J Clin Invest*. 2007;117(7):1884–1892.
46. Vetrano S, et al. The lymphatic system controls intestinal inflammation and inflammation-associated colon cancer through the chemokine decoy receptor D6. *Gut*. 2010;59(2):197–206.
47. Moore RJ, et al. Mice deficient in tumor necrosis factor-alpha are resistant to skin carcinogenesis. *Nat Med*. 1999;5(7):828–831.
48. Svensson M, Irjala H, Svanborg C, Godaly G. Effects of epithelial and neutrophil CXCR2 on innate immunity and resistance to kidney infection. *Kidney Int*. 2008;74(1):81–90.
49. Boisvert WA, et al. Up-regulated expression of the CXCR2 ligand KC/GRO-alpha in atherosclerotic lesions plays a central role in macrophage accumulation and lesion progression. *Am J Pathol*. 2006; 168(4):1385–1395.
50. Boisvert WA, Santiago R, Curtiss LK, Terkeltaub RA. A leukocyte homologue of the IL-8 receptor CXCR-2 mediates the accumulation of macrophages in atherosclerotic lesions of LDL receptor-deficient mice. *J Clin Invest*. 1998;101(2):353–363.
51. Dhomen N, et al. Oncogenic Braf induces melanocyte senescence and melanoma in mice. *Cancer Cell*. 2009;15(4):294–303.
52. Chen Z, et al. Crucial role of p53-dependent cellular senescence in suppression of Pten-deficient tumorigenesis. *Nature*. 2005;436(7051):725–730.
53. Pekarek LA, Starr BA, Toledano AY, Schreiber H. Inhibition of tumor growth by elimination of granulocytes. *J Exp Med*. 1995;181(1):435–440.
54. Shojaei F, Singh M, Thompson JD, Ferrara N. Role of Bv8 in neutrophil-dependent angiogenesis in a transgenic model of cancer progression. *Proc Natl Acad Sci U S A*. 2008;105(7):2640–2645.
55. Youn JI, Nagaraj S, Collazo M, Gabrilovich DI. Subsets of myeloid-derived suppressor cells in tumor-bearing mice. *J Immunol*. 2008;181(8):5791–5802.
56. Houghton AM, et al. Neutrophil elastase-mediated degradation of IRS-1 accelerates lung tumor growth. *Nat Med*. 2010;16(2):219–223.
57. Gregory AD, Houghton AM. Tumor-associated neutrophils: new targets for cancer therapy. *Cancer Res*. 2011;71(7):2411–2416.
58. Balkwill F. Tumour necrosis factor and cancer. *Nat Rev Cancer*. 2009;9(5):361–371.
59. Grivennikov SI, Karin M. Inflammatory cytokines in cancer: tumour necrosis factor and interleukin 6 take the stage. *Ann Rheum Dis*. 2011;1:i104–i108.
60. Coussens LM, Tinkle CL, Hanahan D, Werb Z. MMP-9 supplied by bone marrow-derived cells contributes to skin carcinogenesis. *Cell*. 2000; 103(3):481–490.
61. Chen J, et al. CCL18 from tumor-associated macrophages promotes breast cancer metastasis via PITPNM3. *Cancer Cell*. 2011;19(4):541–555.
62. Tazawa H, et al. Infiltration of neutrophils is required for acquisition of metastatic phenotype of benign murine fibrosarcoma cells: implication of inflammation-associated carcinogenesis and tumor

progression. *Am J Pathol*. 2003;163(6):2221–2232.
63. Kitamura T, et al. Inactivation of chemokine (C-C motif) receptor 1 (CCR1) suppresses colon cancer liver metastasis by blocking accumulation of immature myeloid cells in a mouse model. *Proc Natl Acad Sci U S A*. 2010;107(29):13063–13068.
64. Kitamura T, et al. SMAD4-deficient intestinal tumors recruit CCR1+ myeloid cells that promote invasion. *Nat Genet*. 2007;39(4):467–475.
65. Qian BZ, et al. CCL2 recruits inflammatory monocytes to facilitate breast-tumour metastasis. *Nature*. 2011;475(7355):222–225.
66. Granot Z, Henke E, Comen EA, King TA, Norton L, Benezra R. Tumor entrained neutrophils inhibit seeding in the premetastatic lung. *Cancer Cell*. 2011;20(3):300–314.
67. Huang S, et al. Fully humanized neutralizing antibodies to interleukin-8 (ABX-IL8) inhibit angiogenesis, tumor growth, and metastasis of human melanoma. *Am J Pathol*. 2002;161(1):125–134.
68. Bordon Y, Hansell CA, Sester DP, Clarke M, Mowat AM, Nibbs RJ. The atypical chemokine receptor D6 contributes to the development of experimental colitis. *J Immunol*. 2009;182(8):5032–5040.
69. Sato T, et al. Single Lgr5 stem cells build crypt-villus structures in vitro without a mesenchymal niche. *Nature*. 2009;459(7244):262–265.